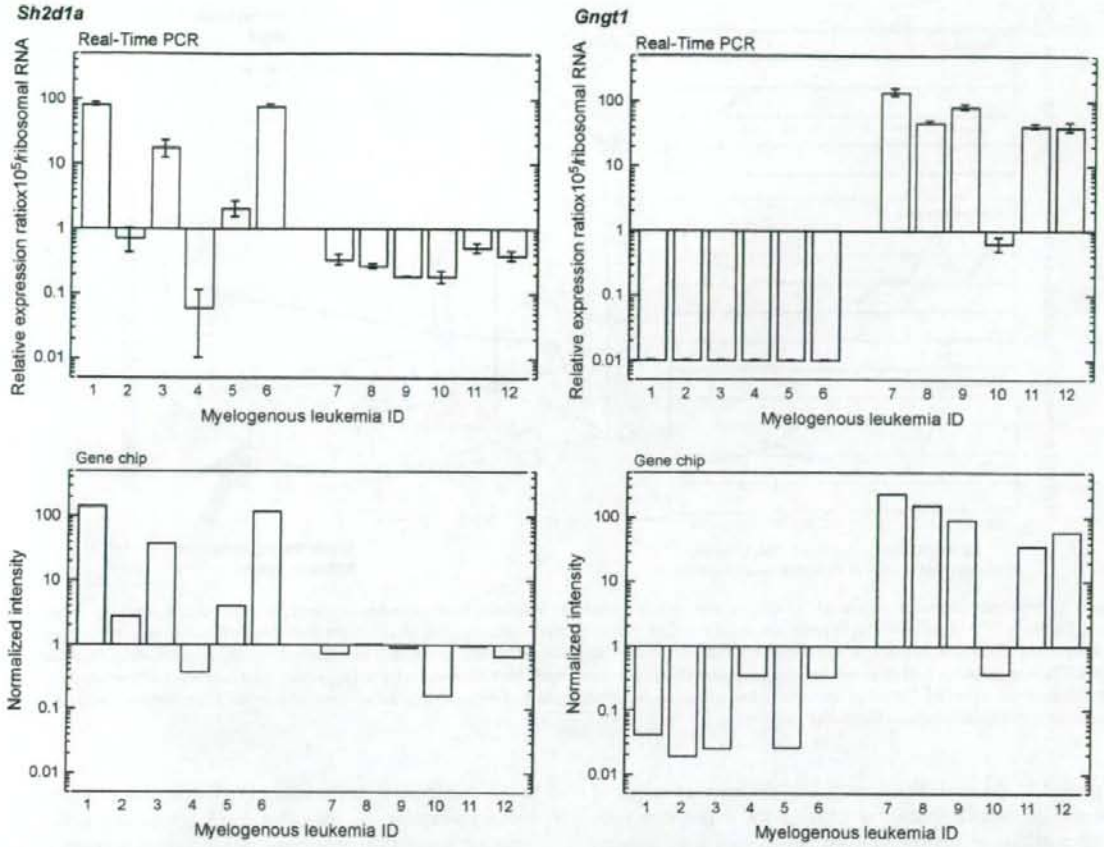

Figure 2. Comparison between the expression ratio of the gene relative to that of ribosomal RNA (top) and relative expression of the gene in the gene chip analysis (bottom) of two genes; *Sh2d1a* and *Gngt1*. The left shows data for *Sh2d1a*, which showed the highest expression intensity in the spontaneous myelogenous leukemia number 1. The right shows those for *Gngt1*, which showed the highest expression intensity in the radiation—induced myelogenous leukemia no. 7 (and no. 12). Similar comparisons between reverse transcriptase polymerase chain reaction (RT—PCR) data and normalized expression obtained by gene chip analysis for the other genes with the highest expression intensity in each of the spontaneous and radiation—induced myelogenous leukemias are shown in Supplementary Figures 1—1 and 1—2, respectively (because of overlap genes, the second highest genes were added). Expression intensity of each gene in each case of myelogenous leukemias (nos. 1 to 12) is shown by a pair of graphs, RT—PCR (top) and gene chip analysis (bottom). The ordinates of the RT—PCR data (top, left and right) indicate relative expression ratio multiplied by 10^5 divided by ribosomal RNA expression, and the ordinates of the gene chip data indicate normalized gene expression intensities in the gene chip analyses.

Comparison of gene expression intensities between genes from mice with spontaneous and radiation-induced myelogenous leukemias

The gene expression profiles of radiation-induced leukemias were relatively homogeneous compared with those of spontaneous leukemias, as shown by the linear configuration (Fig. 1). Thus, because genes with high-expression intensities in each mouse with radiation-induced leukemia were considered to show similar repertoires with similar high-expression intensities, the top 20 genes with the highest expression intensity in each mouse with leukemia were focused on and selected (Table 1A and B; spontaneous and radiation-induced myelogenous leukemias, respectively; also, see Suppl. Tables 1-1 and 1-2 for detail). In Table 1A and B, note that the 20 most expressed genes differ across samples. Of the 120 genes (6 samples × 20 genes) shown in Table 1, 24 genes overlapped 77 times (64%) in two or more samples in the radiation-induced myelogenous leukemia cohort, whereas only 10 genes overlapped 25 times (i.e., as low as 21%) in up to two samples in the six mice with spontaneous myelogenous leukemia cohort. From Tables 1A and B, genes with the highest expression intensity in each of the six mice with spontaneous and six mice with radiation-induced myelogenous leukemias were separately selected and subjected to quantitative RT-PCR analysis (in the case that overlapping genes show the highest expression intensities in other leukemias, genes with the second or third highest expression intensities were

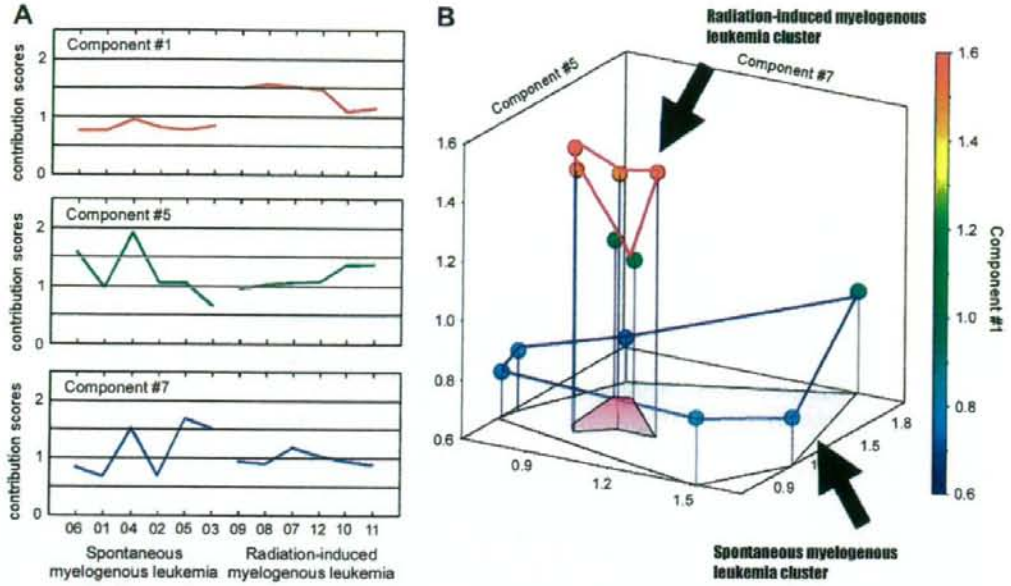

Figure 3. Principal component analysis (PCA) differentiates radiation—induced leukemias from spontaneous leukemias: three—dimensional expression clustering. Results of PCA of six cases each of spontaneous and radiation—induced myelogenous leukemias are shown in the three—dimensional contribution scores for component numbers 1, 5, and 7, which discriminate the radiation—induced myelogenous leukemia cluster from the spontaneous myelogenous leukemia cluster. The line graph on the left shows actual contribution scores converted from each eigenvector value (**A**), which were used for the three—dimensional expression on the right (**B**). Note that the contribution scores of the spontaneous leukemias, except for component number 1, are comparatively divergent from those of radiation—induced leukemias.

subjected to the analysis). Figure 2 shows the expression of two sets of sample genes. For *Sh2d1a*, the expression ratio relative to that of ribosomal RNA determined from spontaneous leukemia number 1 (top left; out of six cases, nos. 1 through 6) is compared with the relative expression intensity of the same gene in the gene chip in the spontaneous myelogenous leukemias (six cases in the bottom left, number 1 through 6). For *Gngt1*, the expression ratio relative to that of ribosomal RNA determined from the radiation-induced myelogenous leukemia number 7 (top right; out of six cases, nos. 7 through 12) is compared with the relative expression intensity of the same gene in the gene chip in the radiation-induced myelogenous leukemias (six cases in the bottom right, nos. 7 through 12).

Sh2d1a expression level was evaluated in not only spontaneous leukemias but also radiation-induced leukemias, and *Gngt1* expression level was evaluated in not only radiation-induced leukemias, but also spontaneous leukemias. Results show that the *Sh2d1a* expression level highly vary in the spontaneous group, whereas it is relatively low, reversed, and homogenous in the radiation-induced group (nos. 7–12); these trends are comparable between the quantitative RT-PCR data (top) and the relative expression intensities in the gene chip analysis (bottom). On the other hand, as shown on the right panels of Figure 2 on the right, the *Gngt1* expression levels are generally high and homogenous, except for that in number 10, in the case of radiation-induced myelogenous leukemias, on the other hand, interestingly, the expression levels in spontaneous myelogenous leukemias are nearly very low. These trends are similar not only between the quantitative RT-PCR data and the relative expression intensities in the gene chip analyses, but also in the expression intensities of the other genes except *Sgip1*, as shown in the radiation-induced myelogenous leukemias examined (see Suppl. Fig. 1). The 24 genes that overlapped in the radiation-induced myelogenous leukemias are shown in Supplementary Table 1-2, which included *G proteins, thrombospondin 4*, and *stem cell growth factor*. None of the 24 genes associated with radiation-induced myelogenous leukemias overlapped with the 10 genes associated with the spontaneous myelogenous leukemia (Suppl. Table 1-1). To confirm the nominal discriminant power of these genes associated with the spontaneous and the radiation-induced myelogenous leukemias, a reference dendrogram based on these 240 genes in total in both leukemias (actually, 170 genes in total after subtraction of the overlapping genes) is shown in Supplementary Figure 2. Based on gene expression intensity, despite the clear discrimination between both myelogenous leukemias, as shown in Supplementary Figure 2, none of the highly expressed genes show any mechanistic discrimination between the gene expressions in the myelogenous leukemia cases.

Table 2. Gene list obtained according to the contribution score of PCA component #1 up to 0.999

Affymetrix systematic name	GenBank ID	Description
1439612_at	AW060892	calcium channel, voltage-dependent, N type, alpha 1B subunit (Cacna1b)
1449476_at	NM_011973	renal tumor antigen (Rage)
1450492_at	NM_013927	cyclic nucleotide gated channel beta 3 (Cngb3)
1422990_at	NM_008591	met proto-oncogene (Met)
1422931_at	NM_008037	fos-like antigen 2 (Fosl2)
1426175_a_at	U42405	mast cell protease 7 (Mcpt7)
1419463_at	AF108501	chloride channel calcium activated 2 (Clca1)
1440134_at	AI647584	Transcribed sequences (Cyp4a10)
1442092_at	BG063268	Fanconi anemia, complementation group D2 (Fancd2)
1427581_at	BI737649	hypermethylated in cancer 2 (Hic2)
1422116_at	NM_008032	fragile X mental retardation 2 homolog (Fmr2)

Spontaneous and radiation-induced myelogenous leukemias are differentiated by PCA

Evaluations by PCA of both myelogenous leukemias are largely defined by component number 1 (Fig. 3A) and further discriminated by the combination of the additional component numbers 5 and 7, as shown in Figure 3B. The entire PCA data of 12 cases are shown in Supplementary Table 2-1. When one analyzes the discriminant components numbers 1, 5, and 7, the radiation-induced myelogenous leukemias are found in one particular cluster in the three-dimensional representation; on the other hand, the spontaneous myelogenous leukemias are separated from the cluster of radiation-induced myelogenous leukemias, but are scattered between the axes of numbers 5 and 7, and the lower axis of number 1.

Whether responsible discriminant genes associated with the two myelogenous leukemia groups form a possible gene cluster that may be relevant to radiation-induced myelogenous leukemogenesis is of interest. Among the genes that contribute to PCA component number 1, 11 genes with contribution scores of >0.99 based on the PCA component number 1 are shown in Table 2. These genes include met proto-oncogene (*Met*), fos-like antigen2 (*Fosl2*), Fanconi anemia, complementation group D2 (*Fancd2*), and fragile X mental retardation 2 homolog (*Fmr2*).

Generation of union gene profiles of each individual gene expression associated with radiation-induced myelogenous leukemias while maintaining inhomogeneity of each gene expression profile

Regardless of the difference between spontaneous and radiation-induced myelogenous leukemias, it takes nearly a lifetime for both myelogenous leukemias to become fatal; i.e., the former ranges from 465 to 636 days, and the latter ranges, in general, from 300 to 800 days, depending on radiation dose. Thus, the profile of each type of myelogenous leukemia may be associated with age-related expression profiles. The extent by which such age-related gene expression profiles overlap with the profiles of myelogenous leukemias is of particular interest, because knowledge of this may help in elucidating more specific gene expressions associated with spontaneous myelogenous leukemia or gene expressions associated with radiation-induced myelogenous leukemias. In Supplementary Figure 3, the linear configurations of genes from the bone marrow of 2-month-old untreated mice (a), 21-month-old -untreated mice (b), mice with spontaneous myelogenous leukemias (c), and mice with radiation-induced myelogenous leukemias (d) are shown from left to right. Strongly expressed genes in untreated 2-month-old mice are expressed less strongly in the mice with radiation-induced leukemias. On the other hand, genes that are expressed less strongly in the steady state in 2-month-old mice are relatively expressed more strongly in mice with radiation-induced leukemias.

To exclude possible age-related factors and to maintain the stochastic and probabilistic expression characteristics of each individual case (rather than an averaged grouping analysis), the profiles of each case of radiation-induced myelogenous leukemia were compared with those of age-related groups as well as with those of spontaneous myelogenous leukemias (data not shown for spontaneous myelogenous leukemias). The procedure for generating union genes is described in the Materials and Methods section. Namely, the gene expression profiles of the 2-month-old and 21-month-old groups were compared separately with each individual expression profile of radiation-induced myelogenous leukemias by PCA, followed by the selection of genes with a contribution score of >1.0 from component numbers 2 or 3 and 6, respectively, based on the results of PCA. Forty-five genes that overlapped with another 249 union genes from the PCA combination between the gene expression profiles of the 21-month-old bone marrow group and each individual expression profile of the spontaneous myelogenous leukemia group were subtracted from the obtained 287 union genes. The union gene list of discriminant gene profiles associated with radiation-induced myelogenous leukemias was then obtained (Suppl. Table 3), which consequently generated a total of 242 genes associated with radiation-induced myelogenous leukemias and included six

Table 3. Sample genes included in the union gene list

Affymetrix systematic name	Common name	Genbank ID	Description
Radiation-effect-related genes			
1425366_a_at	Hus1	AF076845	Hus1 homolog (S. pombe)
1418062_at	Eef1a2	NM_007906	eukaryotic translation elongation factor 1 alpha 2
1419417_at	Vegfc	NM_009506	vascular endothelial growth factor C
Apoptosis/cell-death-related genes			
1419714_at	Pdcd1lg1	NM_021893	programmed cell death 1 ligand 1
1423259_at	Idb4	BB121406	inhibitor of DNA binding 4
1423499_at	Sncaip	AK017012	synuclein, alpha interacting protein (synphilin)
Cell-cycle/cell-growth-related genes			
1421462_a_at	Lepre1	NM_019783	leprecan 1
1425608_at	Dusp3	BC016269	dual specificity phosphatase 3 (vaccinia virus phosphatase VH1-related)
1425750_a_at	Jak3	L40172	Janus kinase 3
Tumor-suppression/tumor-promoter-related genes			
1418597_at	Top3a	NM_009410	topoisomerase (DNA) III alpha
1420034_at	Ppp2r2d	AU019644	protein phosphatase 2, regulatory subunit B, delta isoform
1437307_at	Senp8	BG069815	SUMO/sentrin specific protease family member 8

radiation-related genes including *Hus-1*, *Edf1a2*, and*Vegf-c*; 16 apoptosis/cell-death-related genes including *Pdcd1lg1*, *Ibd4*, and *Sncaip*; 13 cell cycle/cell-growth-related genes including *Lepre1*, *Dusp3*, and *Jac3*; and 50 suppressor/promoter genes including *Topo3a*, *Ppp2r2d*, and *Senp8* (Table 3). Consistently, six mice with radiation-induced and spontaneous myelogenous leukemias were discriminated without supervision with $p < 0.05$ when a mixture of mice with both myelogenous leukemias were examined using a dendrogram of these 242 union genes. No definitive identities of these genes associated with spontaneous myelogenous leukemias, on the other hand, were confirmed because of their pleiotropic bilateral functions in nonproliferative and proliferative cells, with stochastically divergent expression profiles in each case.

Another PCA component differentiates four different eigenvector clusters representing four histopathological findings regardless of either spontaneous myelogenous leukemia or radiation-induced myelogenous leukemia

All the myelogenous leukemia cases analyzed in Figure 1, regardless of either spontaneous or radiation-induced myelogenous leukemia are listed in Supplementary Table 2-2 with descriptions of cytological characteristics and representative pictures shown in Supplementary Figure 4-1. All the data were then rearranged by pathological type, such as two cases with myeloblastic leukemia, two cases with myeloblastic leukemia with erythroid differentiation, four cases with granuloid leukemia and monocytic leukemia, and four cases with myelomonocytic leukemia, in Supplementary Figure 5. On the basis of the PCA results (Suppl. Table 2-1), each eigenvector value associated with the spontaneous and radiation-induced leukemias was not separated but identically grouped unsupervisedly on the basis of component numbers 2, 4, and 6. These eigenvectors representing each pathological diagnostic endpoint were separately located in the three-dimensional representation calculated by PCA (Fig. 4). The gene expression intensities in the four taxonomic groups were significantly different from each other as determined by analysis of variance of the global gene expression profiles (Suppl. Fig. 4-2).

Discussion

In this study, global genes associated with radiation-induced myelogenous leukemias that developed in C3H/He mice were compared with those associated with rare spontaneous myelogenous leukemias that developed in the same strain. These myelogenous leukemias from both origins are essentially indistinguishable neither cytologically nor histopathologically. When one compares the genes associated with both leukemias by linear configuration, a distinct difference between both types of leukemia is observed. Genes associated with spontaneous myelogenous leukemias reveal stochastic and probabilistic divergence in terms of expression intensities and gene combinations. On the other hand, genes associated with radiation-induced myelogenous leukemias reveal more homologous commonalities among the cases possibly owing to the development of such leukemias from limited radiation-fragile sites for initial genomic alterations, although they are still stochastic when one compares them with the expression of steady-state bone marrow cells. The results further show that the expression order of the latter is opposite to that of genes associated with spontaneous myelogenous leukemias. The aim of this study was to elucidate the common characteristic gene repertoires that can identify radiation-specific myelogenous leukemias.

Interestingly, genes strongly expressed in the radiation-induced myelogenous leukemias, as selected from Table 1B

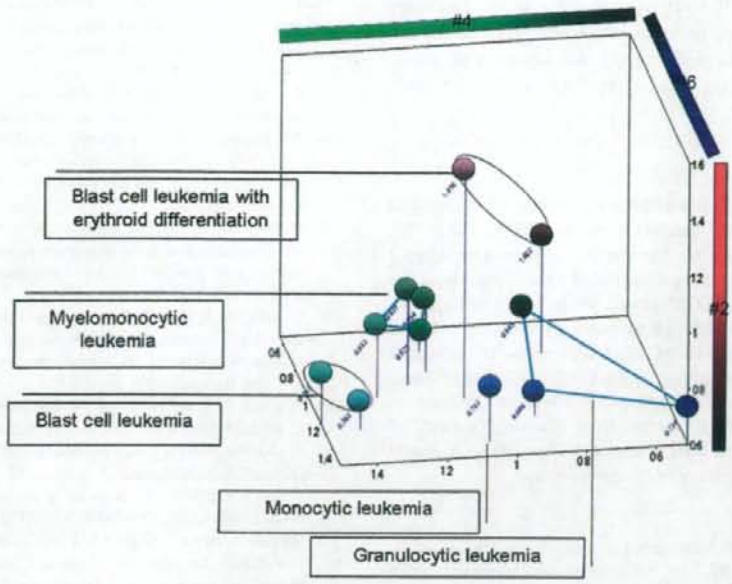

Figure 4. Three—dimensional representation of clusters for each pathological endpoint shown in Supplementary Figure 5. Three different components, namely, numbers 2, 4, and 6, were used from the same principal component analysis data utilized in Figure 3 and Supplementary Table 2.

and Supplementary Table 1-2, showed no radiation-specific gene repertoires, although the genes showed features that can be used to discriminate between spontaneous and radiation-induced myelogenous leukemias (Suppl. Fig. 2). Because the expression profiles of radiation-induced myelogenous leukemias show much stochastic and probabilistic variances, neither expression-intensity-based ordinary dendrographic analysis nor analysis of variance (not presented) can be used to provide responsible gene repertoires.

PCA reduces the size of the space of variables, while preserving most of the variance [20]. It is, therefore, a useful tool for data structure visualization and interpretation. Here, PCA showed a clear discrimination between spontaneous and radiation-induced myelogenous leukemias (Fig. 3) and provided a plausible discriminant gene list. Interestingly, because the expression profiles of radiation-induced myelogenous leukemias show highly stochastic and probabilistic variances, and because PCA is generally applied to explore structure in high-dimensional data, but is not directed towards clustering [10], the inhomogeneous information of each case was not retained during the generalized Procrustes analysis.

In this study, therefore, to retain individual stochasticity, a union gene profile was obtained from each radiation-induced myelogenous leukemia profile and age-matched profiles. These union gene profiles retain individual stochasticities of 242 genes altogether. These seemed to be useful biomarker genes for discriminating radiation-induced myelogenous leukemias from other myelogenous leukemia clusters. These 242 genes can be used to discriminate between the expressions of radiation-induced myelogenous leukemias from those of spontaneous myelogenous leukemia. Interestingly, when these 242 genes were used in an unsupervised manner to determine whether the gene list can be used to discriminate between spontaneous and radiation-induced myelogenous leukemias, both types of leukemia were clearly discriminated by expression intensity, although these are selected from union genes according to individual PCA results, and not by expression intensitiy (Suppl. Fig. 6 A-C). These 242 genes are highly stochastic and probabilistic, thus, have never been introduced previously, but may be useful biomarker genes for clinical use in diagnosis and therapeutics for patients treated by whole-body irradiation.

From the three-dimensional localization of eigenvector data points generated, the histological types of myelogenous leukemia, such as blast cell leukemia and granulomacrophage leukemia can be separately clustered without additional information (Fig. 4). These histo-pathological endpoints indicating responsible gene components, as determined by PCA. They may complement pathological diagnosis based on gene expression as a form of molecular taxonomy. C3H/He mice are prone to develop myelogenous leukemia but generate only 1% spontaneous myelogenous leukemias [2,3]. The incidence of other spontaneous hematopoietic neoplasms was also low as 11.7%. Thus, comparison of gene expression profiles between spontaneous and radiation-induced myelogenous leukemias analyzed in this study is based on a prosperous model, which permits diagnostic confirmation by the pathological characterization. A possible limitation of applicability of present conclusions might be the difficulty in finding such appropriate

experimental models for applying to other areas. The same radiation-induced myelogenous leukemia model under caloric restriction, demonstrating the amelioration of radiation-induced leukemia, has been reported elsewhere [16,21].

Acknowledgments

This study is dedicated to late Eugene P. Cronkite, M.D., Medical Department, Brookhaven National Laboratory, N.Y., U.S.A. We thank Dr. Julian Preston, US Environmental Protection Agency for valuable comments on the manuscript. We also thank Ms. E. Tachihara, Ms. Y. Usami, Ms. Y. Shinzawa, Ms. M. Uchiyama, and Ms. C. Aoyagi for excellent technical assistance, and Ms. Y. Kikuchi, Ms. M. Yoshizawa, and Ms. M. Hojo for secretarial assistance. This work was supported in part by the Human Sciences of Japan (KHC1204), a Grant-in-Aid for Scientific Research C (Numbers 18510066 and 20590388), a fund from Nuclear Research of MEXT, Japan, and also an MHLW Research Fund (H18-Chemistry 0001) of the National Institute of Health Sciences.

References

1. Hirabayashi Y, Inoue T. Toxicogenomics applied to hematotoxicology. Verlag GmbH. In: Borlak J, ed. Handbook of Toxicogenomics. Weinheim: Wiley-VCH; 2005. p. 583–608.
2. Seki M, Yoshida K, Nishimura M, Nemoto K. Radiation-induced myeloid leukemia in C3H/He mice and the effect of prednisolone acetate on leukemogenesis. Radiat Res.. 1991;127:146–149.
3. Yoshida K, Hirabayashi Y, Wada S, et al. p53 (TRP53) deficiency-mediated antiapoptosis escape after 5 Gy X irradiation still induces stem cell leukemia in C3H/He mice: comparison between whole-body assay and bone marrow transplantation (BMT) assay. Radiat Res. 2007;167:703–710.
4. Chaudhry MA. Bystander effect: biological endpoints and microarray analysis. Mutat Res. 2006;597:98–112.
5. Dai JM, Sun DC, Lin RX, Yang J, Lou S, Wang SQ. Microarray analysis of differentially expressed genes in mouse bone marrow tissues after ionizing radiation. Int J Radiat Biol. 2006;82:511–521.
6. Dainiak N, Schreyer SK, Albanese J. The search for mRNA biomarkers: global quantification of transcriptional and translational responses to ionising radiation. BJR Suppl. 2005;27:114–122.
7. Thavathiru E, Ludes-Meyers JH, MacLeod MC, Aldaz CM. Expression of common chromosomal fragile site genes, WWOX/FRA16D and FHIT/FRA3B is downregulated by exposure to environmental carcinogens, UV, and BPDE but not by IR. Mol Carcinog. 2005;44:174–182.
8. Rithidech K, Dunn JJ, Bond VP, Gordon CR, Cronkite EP. Characterization of genetic instability in radiation- and benzene-induced murine acute leukemia. Mutat Res. 1999;428:33–39.
9. Bouffler S, Silver A, Papworth D, Coates J, Cox R. Murine radiation myeloid leukaemogenesis: relationship between interstitial telomere-like sequences and chromosome 2 fragile sites. Genes Chromosomes Cancer. 1993;6:98–106.
10. Guo Q, Wub W, Massart DL, Bouconc C, de Jong S. Feature selection in sequential projection pursuit. Anal Chim Acta. 2001;446:85–96.
11. Schoonjans V, Taylor N, Hudson BD, Massart DL. Characterization of the similarity of chemical compounds using electrospray ionization mass spectrometry and multivariate exploratory techniques. J Pharm Biomed Anal. 2002;28:537–548.
12. Hirabayashi Y, Inoue T. Implications of hemopoietic progenitor cell kinetics and experimental leukemogenesis: relevance to Gompertzean mortality as possible hematotoxicological endpoint. Exp Hematol. 2007;35:125–133.
13. Hirabayashi Y, Inoue T, Suda Y, Aizawa S, Ikawa Y, Kanisawa M. Hemopoietic neoplasms in lethally irradiated mice repopulated with bone marrow cells carrying the human c-myc oncogene: a repopulation assay. Exp Hematol. 1992;20:167–172.
14. Frith CH, Ward JM, Harleman JH, et al. Hematopoietic system. In: Mohr U, ed. International Classification of Rodent Tumors: The Mouse. Berlin: Springer-Verlag Berlin Heidelberg; 2001. p. 417–451.
15. Hirabayashi Y, Matsumura T, Matsuda M, et al. Cell kinetics of hemopoietic colony-forming units in spleen (CFU-S) in young and old mice. Mech Ageing Dev. 1998;101:221–231.
16. Yoshida K, Inoue T, Nojima K, Hirabayashi Y, Sado T. Calorie restriction reduces the incidence of myeloid leukemia induced by a single whole-body radiation in C3H/He mice. Proc Natl Acad Sci U S A. 1997;94:2615–2619.
17. Yoon BI, Li GX, Kitada K, et al. Mechanisms of benzene-induced hematotoxicity and leukemogenicity: cDNA microarray analyses using mouse bone marrow tissue. Environ Health Perspect. 2003; 111:1411–1420.
18. Brazma A, Hingamp P, Quackenbush J, et al. Minimum information about a microarray experiment (MIAME)-toward standards for microarray data. Nat Genet.. 2001;29:365–371.
19. Li GX, Hirabayashi Y, Yoon BI, et al. Thioredoxin overexpression in mice, model of attenuation of oxidative stress, prevents benzene-induced hemato-lymphoid toxicity and thymic lymphoma. Exp Hematol. 2006;34:1687–1697.
20. Massart DL, Kaufman L. The Interpretation of Analytical Chemical Data by the Use of Cluster Analysis. New York: Wiley; 1983.
21. Yoshida K, Hirabayashi Y, Watanabe F, Sado T, Inoue T. Caloric restriction prevents radiation-induced myeloid leukemia in C3H/HeMs mice and inversely increases incidence of tumor-free death: implications in changes in number of hemopoietic progenitor cells. Exp Hematol. 2006;34:274–283.

Supplementary data associated with this article can be found in the online version, at doi:10.1016/j.exphem.2008.10.006

Leukemia Research xxx (2008) xxx–xxx

Contents lists available at ScienceDirect

Leukemia Research

journal homepage: www.elsevier.com/locate/leukres

A novel role for acinus and MCM2 as host-specific signaling enhancers of DNA-damage-induced apoptosis in association with viral protein gp70

Maki Hasegawa [a,b], Morito Kurata [a], Kouhei Yamamoto [a], Kazuko Yoshida [c], Shirou Aizawa [d], Masanobu Kitagawa [a,*]

[a] Department of Comprehensive Pathology, Graduate School, Tokyo Medical and Dental University, 1-5-45 Yushima, Bunkyo-ku, Tokyo 113-8519, Japan
[b] Pharmaceutical Research Division, Takeda Pharmaceutical Company Limited, 10 Wadai, Tsukuba 300-4293, Ibaraki, Japan
[c] Research Center for Radiation Safety, National Institute of Radiological Sciences, 4-9-1 Anagawa, Chiba 263-8555, Japan
[d] Nuclear Safety Technology Center, 5-1-3 Hakusan, Bunkyo-ku, Tokyo 112-8604, Japan

ARTICLE INFO

Article history:
Received 15 August 2008
Received in revised form
22 September 2008
Accepted 27 October 2008

Keywords:
Friend virus
DNA-damage
Apoptosis
Acinus
MCM2
Host-virus relation

ABSTRACT

The interaction of viral proteins with host-cellular proteins elicits the activation of numerous cellular signal transduction pathways possibly leading to the viral pathogenesis. We previously demonstrated that infection with Friend leukemia virus (FLV) radiosensitizes murine hematopoietic cells via a p53-dependent apoptotic pathway in C3H hosts. Here, we show that the transduction of the *env*-gene (gp70) of Friend murine leukemia virus (F-MuLV) sensitized C3H-derived myeloid leukemia cells to DNA-damage (ionizing radiation as well as doxorubicin)-induced apoptosis through the activation of DNA-dependent protein kinase (DNA-PK) and P53. Knockdown of DNA-PK by siRNA inhibited the radiosensitization induced by gp70. In association with gp70 and DNA-PK, the acinus and MCM2 proteins were host-specifically overexpressed in C3H-derived cells. Taken together, these data suggested that gp70 enhances cellular DNA-damage-induced signaling in association with host-specific cellular proteins including acinus and MCM2 resulting in the activation of DNA-PK to phosphorylate P53. This *in vitro* study clearly indicates that the enhancement of DNA-damage-induced apoptosis by gp70 is not caused by the bone marrow environment of the host but is introduced by modified signaling in hematopoietic cells. The mechanisms involved in the ability of a viral protein to regulate cellular gene expression could provide invaluable insight into the manipulation of cellular pro-apoptotic signaling and the development of novel therapeutic strategies.

1. Introduction

Apoptosis is an essential component of the cell response to injury. In particular, many cells will undergo apoptosis following viral infection and this may abort the production and release of virus progeny [1]. It is therefore not surprising that viruses have evolved distinct mechanisms for the modulation of host cell apoptosis. Many host cell factors are known to be used and modified by retroviruses during their life cycle and are potential new targets for therapeutic intervention [2]. Friend leukemia virus (FLV) is a murine retrovirus that can cause splenomegaly and induce erythroleukemia in susceptible strains of mice. Regarding apoptosis and FLV infection, an enhancement of anti-apoptotic signaling has been observed in transformed cell lines [3,4] as well as primary erythroblasts [5]. Recently, an *in vitro* study using an FLV-transformed cell line revealed that the MAPK signaling pathway, which is active in transformed cells, could both positively and negatively influence p53-dependent apoptosis [6]. However, despite this the effects of FLV infection on the pro-apoptotic signaling of infected cells are still controversial.

Ionizing radiation (IR) is widely used to treat a variety of human malignancies. The principal cytotoxic event induced by IR is the DNA double-strand break (DSB) [7]. DNA-damage such as DSB is known to cause p53-dependent apoptosis in many kinds of cells and tissues *in vitro* as well as *in vivo*. One of the upstream activators or the regulators of p53 is known as phosphatidylinositol 3-kinase (PI3K)-related protein kinase (PIKK) family of enzymes [8]. The PIKK family include the ataxia-telangiectasia mutated (ATM), ATM-and Rad3-related (ATR) kinases, and DNA-dependent protein kinase (DNA-PK), which are involved in cell cycle regulation and DNA repair as well [9]. It is clear from the literature that retroviral interactions with the host cell, whether upon initial entry or through successive rounds of replication, often trigger a DNA-damage response, such as the ATM-, or ATR-mediated responses [10–12]. These responses could modify DNA-repair-associated reactions or p53-dependent apoptosis through cellular signaling pathways.

* Corresponding author. Tel.: +81 3 5803 5173; fax: +81 3 5803 0123.
E-mail address: masa.pth2@tmd.ac.jp (M. Kitagawa).

0145-2126/$ – see front matter © 2008 Elsevier Ltd. All rights reserved.
doi:10.1016/j.leukres.2008.10.025

Please cite this article in press as: Hasegawa M, et al. A novel role for acinus and MCM2 as host-specific signaling enhancers of DNA-damage-induced apoptosis in association with viral protein gp70. Leuk Res (2008), doi:10.1016/j.leukres.2008.10.025

Recently, we have clarified that infection with FLV prominently enhances the DNA-damage-induced apoptosis of hematopoietic cells of C3H mice in association with P53, ATM, and DNA-PK [13]. The phenomenon was characterized *in vivo* by severe anemia in host mice when the mice were infected with FLV and then treated with a low dose of total body irradiation (TBI). However, *p53* knockout mice, *ATM* knockout mice, and DNA-PK deficient SCID mice with a C3H background did not exhibit this phenotype. A comparison of apoptotic signals after FLV, TBI, or FLV + TBI treatment of these mice revealed that ATM appeared necessary for introducing signals into the general pathway of TBI-induced apoptosis, while DNA-PK enhanced p53-dependent apoptosis under FLV infection [12,14]. Namely, bone marrow cells from C3H SCID mice exhibited positive signals for p53 activation and an apoptotic response when treated with TBI alone, but did not exhibit enhanced signals when treated with FLV + TBI. Thus, signaling modulation by FLV infection causes participation of DNA-PK in the pathway of apoptosis in response to DNA damage, although DNA-PK is not necessarily essential for the signaling of TBI-induced apoptosis because ATM plays a major role [15].

In association with DNA-PK under FLV infection, an FLV *env*-coding protein (Env), gp70, was co-immunoprecipitated in the bone marrow cell lysate of FLV + TBI-treated C3H hosts [14]. gp70 is a determinant of cell tropism by virtue of its receptor-binding specificity and it mediates the penetration of viral cores into the host cytoplasm [16–18]. Under treatment with FLV + TBI, gp70 protein forms a complex with DNA-PK in the cytoplasm of hematopoietic cells of C3H mice and then DNA-PK demonstrates a strong kinase activity to phosphorylate P53 protein. DNA-PK has been shown to interact with viral proteins in various cases of infection by adenovirus, human cytomegalovirus, and human herpes viruses [19,20]. Furthermore, DNA-PK is known to associate with various proteins which stimulate its catalytic subunit (DNA-PKcs) leading to effective V(D)J recombination and DNA double-strand break repair *in vivo* [21]. Therefore, in addition to other factors that might be involved in the interaction, the function of gp70 as the major enhancing factor that causes DNA-PK to be immediately accumulated and also functions as an active kinase to phosphorylate p53 after DNA-damage, should be precisely determined.

The other key finding *in vivo* was that the enhancement of DNA-damage-induced apoptosis by FLV was only observed in specific strains of mice: C3H and CBA [22]. Thus, host-specific molecules are thought to be involved in this novel pathway of DNA-damage-induced apoptosis. Understanding the role of apoptosis in viral pathogenesis and cytopathicity is greatly facilitated by the availability of an experimental system with both *in vivo* models of disease involving a variety of hosts, and also cell culture models to facilitate a detailed investigation of the apoptosis-related cell signaling pathways [1]. Therefore, the present study was conducted to clarify the precise mechanisms of this enhancement using *in vitro* as well as *in vivo* systems and to reveal the association of viral as well as host (C3H) specific molecules in this pathway.

2. Materials and methods

2.1. Mice and cell lines

Eight to ten-week-old male C3H/HeJ mice (C3H, *H-2*^{k}, *Fv-2*^{s}) were bred from our colony at the Animal Production Facility of the National Institute of Radiological Sciences in Chiba. Specific-pathogen-free DBA/2N (DBA, *H-2*^{d}, *Fv-2*^{s}) mice of 6–8 weeks of age were purchased from the Shizuoka Laboratory Animal Cooperation (Shizuoka, Japan). All of the mice were reared and treated in accordance with the guidelines governing the care and use of laboratory animals at the National Institute of Radiological Sciences (approval numbers 1997–1994 and 1997–1917) and also the guidelines established by the Animal Experiment Committee of the Tokyo Medical and Dental University.

Two clones of radiation-induced myeloid leukemia cell lines derived from C3H mice, 8016 and 8047 cells, were established at the National Institute of Radiological Sciences in Chiba. The cells were cultured in RPMI medium supplemented with 10% fetal bovine serum, penicillin (50 units/ml) (Invitrogen, Carlsbad, CA), and streptomycin (50 μg/ml) (Invitrogen) at 37 °C in an atmosphere of 5% CO_2 in air. It has been confirmed that these cells express myeloid cell marker, Gr-1 and do not harbor mutation or deletion of the p53 gene.

2.2. Viral infection and DNA-damage-induction

An NB-tropic Friend leukemia virus complex, originally from Dr. C. Friend, was prepared as described earlier [23] and was incubated with cells that had been seeded 24 h previously at a highly leukemogenic dose of 10^4 PFU/dish [24]. On day 7 after incubation with FLV, the cells were treated with 3 Gy of irradiation (IR). A dose of 3Gy IR was delivered from a GAMMA-CELL-40 at a dose rate of 1.12 Gy/min. Where indicated, the cells were pretreated with 2 μM wortmannin 24 h before irradiation. Similarly, the cells were treated with 5 μM doxorubicin (Sigma, St. Louis, CA) on day 7 after incubation with FLV. For the *in vivo* studies, the same dose of FLV was injected i.p. into mice, and total body irradiation (3 Gy) was performed as described previously [13].

2.3. Detection of apoptotic cells

To detect the ratio of apoptotic cells after the treatments with FLV, IR, wortmannin, doxorubicin, or siRNA, cells were collected, washed with ice-cold PBS, and fixed with 4% paraformaldehyde solution for 20 min. After washing them with ice-cold PBS, the cells were incubated in 0.1% sodium citrate-0.1% Triton X-100 for 2 min, washed with ice-cold PBS, and then, incubated with FITC-labeled dUTP and TdT at 37 °C for 60 min. Finally, 500 μl of 1% paraformaldehyde solution was added to cell pellets and the samples were analyzed on a FACScan flow cytometer (Becton Dickinson Immunocytometry Systems, Mountain View, CA).

2.4. Immunoprecipitation and immunoblotting analysis

Cell lysates were prepared by incubating cell pellets on ice for 15 min in ice-cold lysis buffer containing 10 mM Tris–HCl, pH 7.5, 5mM EDTA, 1% Nonidet P-40, 0.02% NaN_3, 1 mM PMSF, 0.1% aprotinin, 100 μM leupeptin and 100 μM TPCK (Sigma). The supernatants were separated from debris by centrifugation at 12,000 rpm for 5 min at 4 °C. Protein concentrations were determined using a Bio-Rad protein assay kit (Bio-Rad Laboratories, Hercules, CA). Cell lysates which contained 100 μg of protein were incubated with antibodies and protein A-sepharose beads (Amersham Life Science, Buckinghamshire, England). The resulting immunoprecipitates after centrifugation or whole cell lysates of 50–100 μg were subjected to 6–12.5% SDS-PAGE. Gels were transferred electrophoretically to nitrocellulose membranes (Schleicher and Schull, Dassel, Germany). The membranes were blocked with 10% skimmed milk in PBS, incubated with primary antibodies, and after being washed, were incubated with peroxidase-conjugated secondary antibodies. Bands in the washed membrane were detected with an enhanced chemiluminescence (ECL) system (Amersham Life Science) as described previously [17].

2.5. Antibodies

Mouse monoclonal anti-p53 antibody Pab421 (Oncogene Research Product, Cambridge, MA), rabbit polyclonal anti-phosphor-p53 (Ser15) antibody (Cell Signaling Technology Inc., Beverly, MA), and anti-actin antisera (Sigma) were used for immunoblotting. The mouse monoclonal anti-DNA-PK antibody (Neo Markers, San Jose, CA) was used for immunoprecipitation. The goat polyclonal anti-Moloney MuLV gp70 antibody (Quality Biotech, Camden, MJ), which is known to cross-react with F-MuLV gp70 [17] was used for immunoprecipitaion and as the primary antibody for immunoblotting. The goat polyclonal anti-acinus antibody (sc-5428) (Santa Cruz Biotechnology, Santa Cruz, CA) and anti-MCM2 antibody (sc-9839) (Santa Cruz) were also used for immunoblotting. Horseradish peroxidase-conjugated anti-mouse IgG antibody (Dakopatts, Glostrup, Denmark), horseradish peroxidase-conjugated anti-rabbit IgG antibody (Dakopatts), and horseradish peroxidase-conjugated anti-goat IgG antibody (Dakopatts) were used as secondary antibodies for immunoblotting.

2.6. Kinase assay

Kinase assays were performed according to the protocol of Shangary et al. [25] with our modifications [14]. Cell lysates were incubated with anti-DNA-PK for 2 h on ice and then, mixed with 25 μl of protein A-sepharose beads rocking at 4 °C for 1 h. The immunoprecipitates obtained with the anti-DNA-PK antibody were centrifuged, washed three times, and used for the kinase assays. The immunoprecipitate was mixed with the substrate, 1 μg of p53 protein (p53 (1–393), Santa Cruz), and 5 μM of cold ATP in kinase buffer (50 mM HEPES, pH 7.5, 100 mM KCl, 10 mM $MgCl_2$, 0.2 mM EGTA, 0.1 mM EDTA, and 1 mM dithiothreitol). The kinase reaction was carried out at room temperature for 30 min and was terminated by adding an equal volume of SDS sample buffer followed by heat inactivation. The reaction products were subjected to 10% SDS-PAGE and transferred onto a nitrocellulose membrane. The membrane was

Please cite this article in press as: Hasegawa M, et al. A novel role for acinus and MCM2 as host-specific signaling enhancers of DNA-damage-induced apoptosis in association with viral protein gp70. Leuk Res (2008), doi:10.1016/j.leukres.2008.10.025

processed for immunoblotting using the phospho-p53 (Ser15) antibody as described above and then, analyzed.

2.7. Transfection of gp70

To determine the effect of viral protein on radiosensitivity, we generated stable cell lines in which FLV gp70 was constitutively and stably expressed in 8016 or 8047 cells. In brief, the Friend MuLV gp70 cDNA fragment was cloned into the expression vector pMV12 containing a neomycin resistance gene. The resulting pMV12-gp70 construct was used for transfection. The gp70-transfected cells were maintained under antibiotic selection to retain the gp70 using G-418 sulfate (Invitrogen) at a final concentration of 500 μg/ml.

2.8. Transfection of small-interfering RNA (siRNA)

RNA interference was used to silence DNA-PK gene expression in the 8016 and 8047 cells. The cells were plated in 6-well culture dishes with complete medium (2.5×10^4 cells/well) and allowed to grow for 24 h so as to reach 50–80% confluence. The cells were then transfected with a 21-nucleotide small-interfering RNA (siRNA) (20 pmol) for targeting of DNA-PK mRNA using LipofectAMINE 2000 (Invitrogen) according to the manufacturer's instructions. The sequence of the siRNA used was GCAGGACACTCAGAACGCACTATTA. An irrelevant siRNA that does not lead to the specific degradation of any cellular mRNA was used as a negative control whose sequence was GCACACAGACTGCAATCACAGGTTA. Specific silencing of the targeted gene by small interference RNA (siRNA) was monitored by reverse transcription (RT)-PCR 24 h after transfection. Briefly, total RNA isolated from 8016 or 8047 cells using Trizol reagent (Invitrogen) according to the manufacturer's directions was reverse transcribed with Random Hexamers, and the PCR reaction was performed. Oligonucleotides were synthesized as specific primers for DNA-PK by a commercial laboratory (Life Technologies Oriental, Tokyo, Japan). The sequences of the primers were as follows: DNA-PK: 5′PCR primer CAAGGAACCACCCACCAAA, 3′PCR primer TTGCTACGGATCACATATGGC; β-actin: 5′PCR primer TGGAATCCTGTGGCATCCATGA, 3′PCR primer ATCTTCATGGTGCTAGGAGCCAG. The expected sizes of the PCR products were 188 bp for DNA-PK and 175 bp for β-actin.

2.9. Densitometric analysis

The densities of bands were measured by densitometric analysis with an ImageQuant scanning imager (Molecular Dynamics, Sunnyvale, CA, USA). The relative intensities of the bends were calculated by comparing the density of the sample with that of the control.

2.10. MALDI-TOF mass spectrometry

The protein bands were cut out of Coomassie Brilliant Blue stained gels using a cutter, and then washed three times with Milli-Q water. The gels were destained with 25 mM ammonium hydrogen carbonate in 50% acetonitrile (ACN) for 10 min and dehydrated with ACN for 5 min. Then, the reduction solution containing 10 mM EDTA was added and incubated with 10 mM DTT and 50 mM ammonium hydrigen carbonate in DW at 65 °C for 1 h. After evaporating off the solution, the alkylate solution containing 10 mM EDTA and 40 mM Iodoacetamid was added. The gel pieces were dried in a vacuum, and the proteins were digested overnight in 10 ml trypsin (10 ng/ml, Trypsin Gold, mass spectrometry grade, Promega, Madison, WI) in 25 mM ammonium bicarbonate at 37 °C. Tryptic peptides were lyophilized and resuspended in 2 μl matrix solution containing 10 mg/ml α-cyano-4-hydroxycinnaminc acid (CHCA) prepared in 50% ACN/0.1% TFA, and 0.7 μl of the sample was spotted onto the MALDI sample target plate. Peptide mass spectra were obtained in a MALDI-TOF/TOF mass spectrometer (Voyager DE-STR, Applied Biosystems, Foster, CA). Before the real sample acquisition, six calibrated spots were used for signal and parameter optimization. Peptide mass fingerprinting (PMFs) was obtained in the mass range between 800 and 4000 Da with approximately 5000 laser shots. To obtain the spectra with a low mass accuracy, trypsin and adrenocorticotropic hormone peaks were used for internal calibration of the mass spectra. Protein identification was processed and analyzed by searching the Swiss-Prot and NCBI non-redundant protein sequence databases using the MS-Fit search of Matrix Science that is integrated in the Global Protein Server (GPS) Workstation.

3. Results

3.1. Enhancement of IR-induced apoptosis in FLV-infected myeloid cell lines

To investigate whether infection with FLV actually enhances DNA-damage-induced apoptosis in the *in vitro* system, 8016 or 8047 cells, a C3H-derived myeloid leukemia cell line, were infected with FLV and then irradiated (3 Gy). After infection with FLV, more than

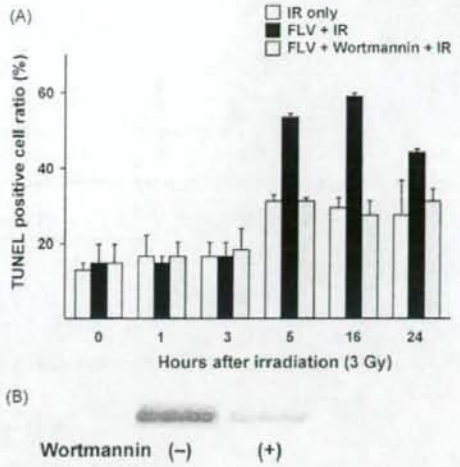

Fig. 1. The effects of IR, FLV and wortmannin treatments on the apoptotic cell ratio of murine leukemia cell line cells. (A) Temporal kinetics of the TUNEL positive cell ratio of 8047 cells after treatment with IR (white column), FLV + IR (black column), or FLV + wortmannin + IR (grey column). Note the remarkable enhancement of apoptosis in the FLV + IR-treated cells as compared with the IR only-treated cells 5–24 h after IR. The treatment with wortmannin showed complete suppression of the enhancement of IR-induced apoptosis by FLV infection. (B) Kinase assay showing the inhibition of DNA-PK activity by wortmannin in IR-treated 8047 cells.

80% of cells expressed gp70 antigen on the cell surface of these cell line cells determined by flow cytometry. Fig. 1A shows the apoptotic cell ratio of 8047 cells as determined by a TUNEL assay after treatment with IR only and FLV + IR. As shown here, FLV + IR-treatment (black column) induced a significantly higher frequency of apoptosis in the 8047 cells as compared with the IR only-treatment (white column) 5, 16, and 24 h after IR. To clarify the contribution of DNA-PK to the enhancement of IR-induced apoptosis, wortmannin, a specific inhibitor of PIKK family enzymes, was administered before IR. The wortmannin treatment clearly reduced the kinase activity of DNA-PK in the IR-treated 8047 cells (Fig. 1B) as determined by the kinase assay. As shown in Fig. 1A, the treatment totally inhibited the enhanced apoptosis in the FLV + IR-treated 8047 cells (grey column) indicating that the PIKK enzyme plays a key role in the enhancement of IR-induced apoptosis by FLV. Although the data were not shown, the 8016 cells exhibited a similar response. However, as the wortmannin is not a specific inhibitor of DNA-PK, modification of other signaling pathways via the effects of PIKK family enzymes could not be ruled out.

Next, to determine the status of p53 after FLV + IR treatment in leukemia cells, the expression dynamics of the p53 and phospho-p53 proteins were analyzed by Western blotting. As shown in Fig. 2A, the expression levels of p53 and phospho-p53 were slightly up-regulated 3 and 6 h after IR in the 8016 cells. By contrast, FLV infection strongly enhanced the over-expression and activation of p53 in these cells. The kinase assay of DNA-PK was performed using immunoprecipitation with anti-DNA-PK antibody and additional p53 protein as the substrate. As shown in Fig. 2B, the kinase activity of DNA-PK was also up-regulated after FLV + IR treatment. Similar to the data shown in the previous *in vivo* study [14], co-immunoprecipitation of gp70 with DNA-PK was identified in FLV + IR-treated cells 3–13 h after IR (Fig. 2C), although low level of endogenous gp70 protein was detected in FLV (–) 8016 cells. These results indicate that the C3H mice-specific *in vivo* enhancement of total body irradiation-induced apoptosis after FLV infection

Please cite this article in press as: Hasegawa M, et al. A novel role for acinus and MCM2 as host-specific signaling enhancers of DNA-damage-induced apoptosis in association with viral protein gp70. Leuk Res (2008), doi:10.1016/j.leukres.2008.10.025

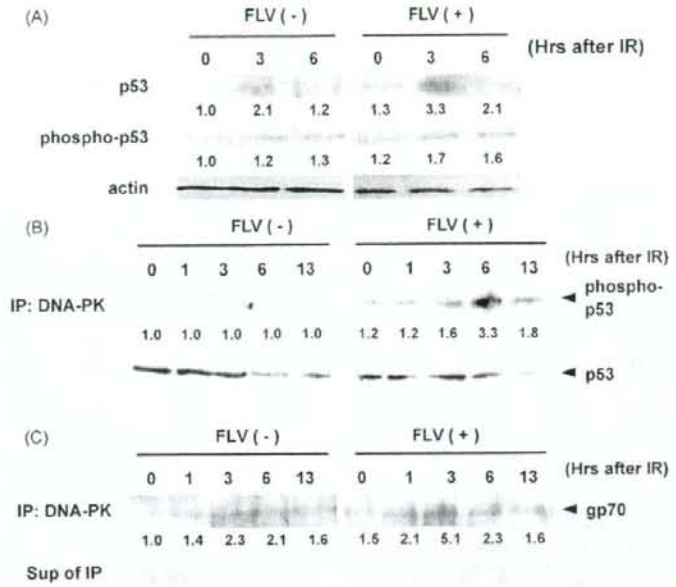

Fig. 2. Chronological changes in the expression and immunoprecipitation analysis of apoptosis-associated molecules in 8016 cells with or without FLV infection after IR. (A) Immunoblotting for p53 protein and phospho-p53 protein in 8016 cells 0, 3, and 6 h after IR (3 Gy). Cell lysates were prepared from the FLV (−) or FLV (+) cells. As the bands for actin protein exhibited a similar density in each sample, the amount of protein contained in cell lysates was similar in each lane. The FLV-infected 8016 cells revealed marked over-expression of p53 protein as well as phopspho-p53 3–6 h after IR, although FLV (−) cells also induced a slight increase of p53 and phopspho-p53 expression. The relative intensities of bands were measured by densitometry (0 h, FLV (−) as the control, 1.0) and indicated under the photos of gels. (B) Kinase assays for DNA-PK from the FLV (−) or FLV (+) 8016 cells 0, 3, 6, and 13 h after IR (3 Gy). Cell extracts were prepared from the FLV (−) or FLV (+) cells. Immunoprecipitates for DNA-PK were prepared by mixing equal amounts of lysate with anti-DNA-PK antibody. The kinase activity of each immunoprecipitate that would phosphorylate recombinant human p53 protein at Ser15 *in vitro* was assessed by immunoblotting for phospho-p53 protein. The same samples after the kinase reaction were also assayed to measure the amount of total p53 protein by immunoblotting. Note the prominent signals for phospho-p53 in the FLV (+) 8016 cells at 6–13 h in the DNA-PK immunoprecipitate. The total amount of p53 protein in the DNA-PK immunoprecipitates was similar in each experimental group. The relative intensities of bands were measured by densitometry (0 h, FLV (−) as the control, 1.0) and indicated under the photos of gels. (C) Co-immunoprecipitation analysis for DNA-PK with FLV-associated protein detected using anti-Moloney MuLV gp70 antibody, which is known to cross-react with Friend MuLV gp70. Note that the gp70 protein was strongly co-immunoprecipitated with DNA-PK in the FLV (+) 8016 cells at 3–13 h after IR. Supernatants of the immunoprecipitates were also immunoblotted for gp70 confirming that the gp70 molecule was immunoprecipitated with the anti-DNA-PK antibody. Although the viral protein was also detected in the FLV (−) mice, these weak signals would indicate the cross-reaction of this antibody with endogenous viral proteins. The relative intensities of bands were measured by densitometry (0 h, FLV (−) as the control, 1.0) and indicated under the photos of gels.

[13] and the associated modification of signaling molecules [14] could be quite similarly demonstrated in an *in vitro* experimental system using C3H-derived myeloid leukemia cell lines. Therefore, the mechanisms included in the enhanced apoptosis by FLV were attributable to hematopoietic cells and not to bone marrow microenvironment interactions such as with stromal cells or humoral factors.

3.2. Enhancement of IR-induced apoptosis in the cells transfected with gp70 of FLV and analysis of associated molecules

After infection with FLV, TBI-induced apoptosis was enhanced in association with p53, DNA-PK, and FLV gp70 in the *in vivo* system [14]. Thus, to investigate whether gp70 alone can enhance p53-dependent IR-induced apoptosis via DNA-PK activation of hematopoietic cells, we constructed an *in vitro* transfection system using the C3H-derived 8016 leukemia cell line. First, the expression of the gp70 protein was confirmed in FLV-infected (Fig. 3A, lane 2) and gp70-transfected cells (Fig. 3A, lanes 3–5). Among several gp70-transfected cell lines, the most prominent expression was achieved in the 8016 F1 cells (Fig. 3A, lane 5), therefore, these cells were used in the following experiments. Then, apoptotic cells were identified in the 8016 parent cells and 8016 F1 cells using the TUNEL method 6 h after IR treatment. As shown in Fig. 3B, when the cells were treated with IR, the 8016 parent cells exhibited a slight increase in the TUNEL positive cell ratio (white column), while the 8016 F1 cells showed a prominent increase of apoptotic cells after IR treatment (light grey column).

As shown in Fig. 3C, the expression levels of p53 and phospho-p53 were prominently up-regulated 3 and 6 h after IR in the 8016 F1 cells. Furthermore, co-immunoprecipitation of DNA-PK with gp70 was identified in the IR-treated 8016 F1 cells 3 to 6 h after IR. These results indicate that the transduction of gp70 to C3H-derived cells alone could introduce the enhancement of IR-induced apoptosis and the associated modification of signaling molecules in the *in vitro* system.

3.3. Knockdown experiments of DNA-PK by siRNA

To examine the contribution of DNA-PK to the enhancement of IR-induced apoptosis in 8016 F1 cells, knockdown experiments were performed using siRNA against DNA-PK. As shown in Fig. 3D, the expression of mRNA for DNA-PK was clearly inhibited after treatment with siRNA. Although the data are not shown, Western blot analysis also revealed the specifically blocked expression of DNA-PK by siRNA at the protein level. The TUNEL assay (Fig. 3B) demonstrated that siRNA-treatment against DNA-PK completely inhibited the enhancement of IR-induced apoptosis in the 8016 F1 cells (black column), namely, the apoptotic cell ratio of the

Please cite this article in press as: Hasegawa M, et al. A novel role for acinus and MCM2 as host-specific signaling enhancers of DNA-damage-induced apoptosis in association with viral protein gp70. Leuk Res (2008), doi:10.1016/j.leukres.2008.10.025

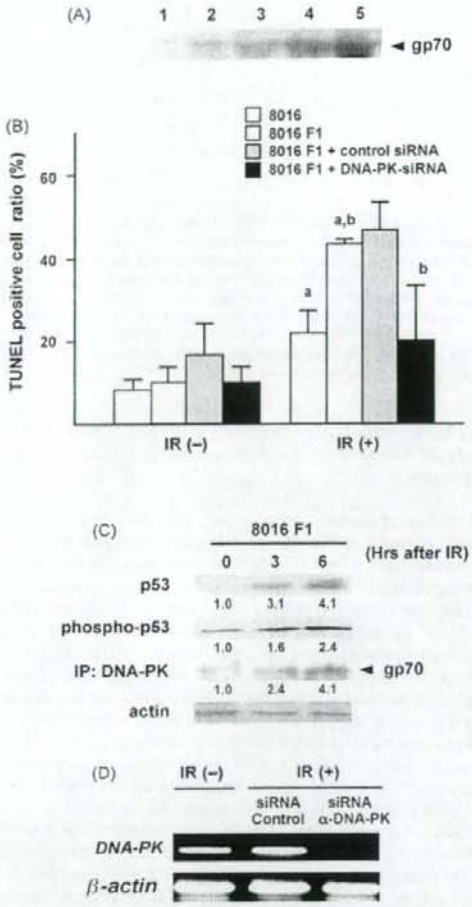

Fig. 3. The effects of gp70 transfection to 8016 cells on IR-induced apoptosis. (A) Expression analysis of transfected gp70 in 8016 cells. Cell lysates were immunoblotted with anti-gp70 antibody for 8016 parent cells (lane 1), FLV-infected 8016 cells (lane 2), gp70-transfected 8016 A1 cells (lane 3), gp70-transfected 8016 C1 cells (lane 4), and gp70-transfected 8016 F1 cells (lane 5). (B) IR-induced apoptosis determined by TUNEL assay in 8016 cells (white column), 8016 F1 cells (light grey column), 8016 F1 cells + negative control siRNA (dark grey column), and 8016 F1 cells + anti-DNA-PK siRNA (black column) 6 h after IR. Note the remarkable enhancement of IR-induced apoptosis in the 8016 F1 cells as compared with that in the 8016 parent cells. The treatment with anti-DNA-PK siRNA clearly inhibited the enhancement of IR-induced apoptosis in 8016 F1 cells, while the treatment with negative control siRNA evoked no marked change. Differences were significant between the ratio of IR-treated 8016 parent cells and that of IR-treated 8016 F1 cells ($^{a}p < 0.05$) and between the ratio of IR-treated 8016 F1 cells and that of IR-treated and anti-DNA-PK siRNA-treated 8016 F1 cells ($^{b}p < 0.01$) by Student's *t*-test. (C) Immunoblotting for p53 protein and phospho-p53 protein and co-immunoprecipitation analysis for DNA-PK with gp70 in 8016 F1 cells 0, 3, and 6 h after IR (3 Gy). The relative intensities of bands were measured by densitometry (0 h, 8016 F1, as the control, 1.0) and indicated under the photos of gels. (D) RT-PCR analysis for DNA-PK mRNA showing specific silencing of DNA-PK expression by siRNA.

IR-treated 8016 F1 cells reduced to that of the IR-treated 8016 parent cells by siRNA-treatment. The treatment with negative control siRNA did not evoke remarkable changes in the TUNEL positive cell ratio of 8016 F1 cells after IR (dark grey column) as compared with the IR-treated 8016 F1 cells (light grey column).

3.4. Apoptotic induction by DNA-damage introduced by doxorubicin-treatment in gp70-transfected leukemia cells derived from C3H

DNA-damage is known to be induced not only by IR but also by several chemical agents such as doxorubicin. Thus, to test whether the apoptotic signaling pathway was activated by chemically induced DNA-damage in gp70-transfected cells, the 8016 F1 cells were treated with doxorubicin and the expression of p53 and phospho-p53, as well as the kinase activity of DNA-PK, and the co-immunoprecipitaion assay of gp70 with DNA-PK were determined. As shown in Fig. 4A, the treatment with doxorubicin caused a very mild increase in the TUNEL positive cell ratio in the 8016 cells (white column). As expected, the 8016 F1 cells exhibited a significantly higher ratio of TUNEL positive cells after IR (grey column).

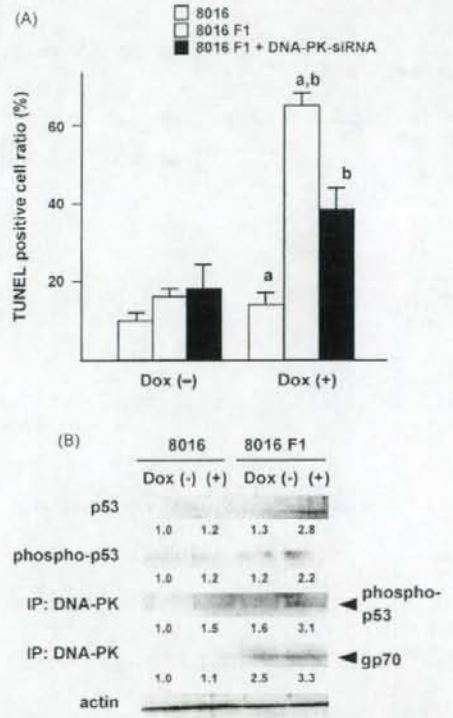

Fig. 4. Induction of apoptosis by doxorubicin in leukemia cells. (A) The apoptotic cell ratio determined by TUNEL assay in 8016 parent cells (white column) and gp70-transfected 8016 F1 cells (grey column) 6 h after treatment with doxorubicin. Note the significant enhancement of doxorubicin-induced apoptosis in the 8016 F1 cells as compared with the 8016 parent cells. The knockdown experiments were performed similarly to the experiments in Fig. 3A. The treatment with siRNA against DNA-PK partially inhibited the enhanced apoptosis induced by doxorubicin in the 8016 F1 cells (black column). Differences were significant between the ratio of doxorubicin-treated 8016 parent cells and that of doxorubicin-treated 8016 F1 cells ($^{a}p < 0.01$) and between the ratio of doxorubicin-treated 8016 F1 cells and that of doxorubicin-treated and anti-DNA-PK siRNA-treated 8016 F1 cells ($^{b}p < 0.01$) by Student's *t*-test. (B) Immunoblotting for p53 protein and phospho-p53 protein, kinase assay for DNA-PK, and co-immunoprecipitation analysis for DNA-PK with gp70 in 8016 parent cells and 8016 F1 cells. Note the up-regulation of p53 expression, p53 activation, DNA-PK activity, and the co-immunoprecipitation of DNA-PK with gp70 in 8016 F1 cells after treatment with doxorubicin. The relative intensities of bands were measured by densitometry (8016, Dox (–), as the control, 1.0) and indicated under the photos of gels.

Please cite this article in press as: Hasegawa M, et al. A novel role for acinus and MCM2 as host-specific signaling enhancers of DNA-damage-induced apoptosis in association with viral protein gp70. Leuk Res (2008), doi:10.1016/j.leukres.2008.10.025

The knockdown experiments with siRNA against DNA-PK partially inhibited the enhanced apoptosis caused by doxorubicin in the 8016 F1 cells (black column). Fig. 4B shows the enhanced expression of phospho-p53 as well as the higher kinase activity of DNA-PK in doxorubicin-treated 8016 F1 cells than in doxorubicin-treated 8016 parent cells. Although the association of gp70 with DNA-PK was identified in doxorubicin-treated 8016 F1 cells, the constitutive over-expression of gp70 in 8016 F1 cells masked the doxorubicin-specific reaction in these cells. Further study should clarify the mechanism for constitutive association of gp70 and DNA-PK.

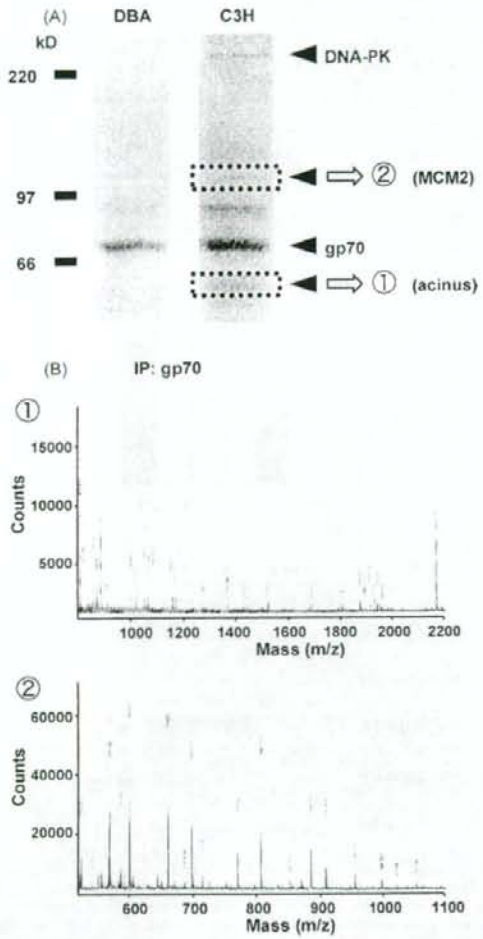

Fig. 5. Analysis of host (C3H) specific molecules enhancing the DNA-damage-induced apoptosis using MALDI-TOF mass spectrometry. (A) Bone marrow cell lysates were prepared from FLV-infected and TBI-treated (3 Gy) DBA and C3H mice. Then, the samples were immunoprecipitated against anti-gp70 antibody. The precipitates were denatured and separated on SDS-polyacrylamide gels, followed by staining with Coomassie Brilliant Blue. In DBA and C3H samples, gp70 protein was identified with a molecular weight around 70 kDa. By contrast, several bands were determined only in the bone marrow sample from C3H. They include two fragments (① and ②) other than DNA-PK protein. These two proteins were removed for identification by MALDI-TOF mass spectrometry. (B) The representative MALDI-TOF peptide mass fingerprints of the tryptic digests corresponded to acinus (①) and MCM2 (②). The demonstrated peptides sequences matched well with those of acinus or MCM2 as determined by GPS Workstation.

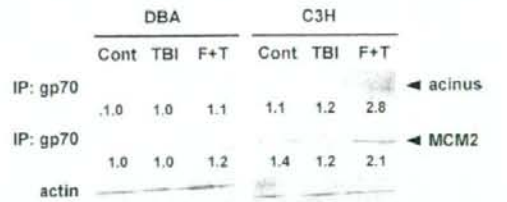

Fig. 6. Immunoblotting for acinus and MCM2 proteins in the immunoprecipitates against anti-gp70 antibody of bone marrow cells from DBA and C3H mice 6 h after TBI (3 Gy). Cell lysates were prepared from the bone marrow of control mice, TBI-treated mice and mice with FLV infection followed by TBI-treatment (F+T) and then, were immunoprecipitated with anti-gp70 antibody. The precipitates were immunoblotted for acinus and MCM2. Note the over-expression of acinus and MCM2 proteins in bone marrow samples from F+T-treated C3H mice but not in samples from DBA mice. The relative intensities of bands were measured by densitometry (DBA, Cont. as the control, 1.0) and indicated under the photos of gels.

3.5. *Analysis for the factors specifically expressed in bone marrow cells of C3H mice after FLV and TBI treatment by MALDI-TOF mass spectrometry*

To determine the molecules associated with the host (C3H) specific enhancement of DNA-damage-induced apoptosis by FLV, bone marrow cell lysates from FLV+TBI-treated DBA and C3H mice were immunoprecipitated with anti-gp70 antibody and the precipitates were electrophoresized and stained with Coommassie Brilliant Blue. Then, two bands that were specifically identified in the sample from C3H bone marrow, circa 50 kDa and 120 kDa (Fig. 5A ① and ②), respectively, were cut out, digested with trypsin, and analyzed by MALDI-TOF mass spectrometry. Two representative spectra of two peptides are shown in Fig. 5B. One peptide from a band with a molecular weight of about 50 kDa (①) showed a partial identity with an apoptotic chromatin condensation inducer in the nucleus (acinus) (GenBank accession no. Q9JIX8). Another peptide from a band with a larger size (②) was identified as minichromosome maintenance protein 2 (MCM2) (GenBank accession no. P97310).

Then, to confirm that the acinus and MCM2 proteins were actually expressed and associated with the gp70 protein in the bone marrow of C3H mice after FLV+TBI-treatment, immunoprecipitaion with anti-gp70 antibody followed by immunoblot analysis using anti-acinus and anti-MCM2 antibodies was performed. The expression levels of these proteins were compared between bone marrow cell samples from DBA and C3H mice. As shown in Fig. 6, bands for acinus as well as MCM2 proteins were specifically observed in the immunoprecipitates of the samples from FLV+TBI-treated C3H bone marrow cells against anti-gp70 antibody, although the MCM2 protein was constitutively expressed in control C3H sample. On the contrary, bone marrow cells from FLV+TBI-treated DBA mice did not exhibit a marked association of acinus and MCM2 proteins with gp70 protein.

4. Discussion

Apoptotic cell death forms part of the host defense against viral infection. Therefore, many viruses inhibit apoptosis to prevent premature cell death and then increase viral progeny production in the cell. This process might generate cellular resistance against various types of apoptosis. For example, the orf virus, a member of the poxvirus family, is known to inhibit apoptosis by encoding a Bcl-2-like protein, which induces full resistance to UV-induced changes in cell morphology, caspase activation, and DNA fragmentation [26]. Similarly, small DNA tumor viruses such as adenovirus, simian virus 40, and high risk human papilloma viruses have vari-

Please cite this article in press as: Hasegawa M, et al. A novel role for acinus and MCM2 as host-specific signaling enhancers of DNA-damage-induced apoptosis in association with viral protein gp70. Leuk Res (2008), doi:10.1016/j.leukres.2008.10.025

ous kinds of tools to inactivate p53. These mechanisms can inhibit p53-mediated apoptosis and help these viruses to maintain oncogenic processes [27]. In the case of HTLV-I, the oncogenic potential of Tax protein is believed to depend on both its ability to alter the expression of the cellular genes involved in cell growth and proliferation, and its direct interaction with cell cycle regulators [28]. Actually, Tax expression promotes anti-apoptotic processes in T cells [29].

By contrast, some viruses are known to induce apoptosis to enhance viral progeny transmission and avoid immune responses [27,30]. Recent studies have demonstrated examples of retrovirus-induced pro-apoptotic cellular responses. The murine leukemia virus envelope protein gPr80env of mink cell focus-forming virus (MCFV) is shown to induce endoplasmic reticulum stress and apoptosis in mink epithelial cells [31]. However, in a part of MCFV-infected cells, up-regulation of the cellular protein c-IAP1 occurs at the translational level. The inhibitor of apoptosis (IAP) family proteins has strong anti-apoptotic effects and therefore chronically MCFV-infected cells survive apoptosis and undergo tumorigenic processes. Thus, the studies on MCFV provide evidence for the biphasic effects of viral infection on apoptosis indicating that the ability of a simple retrovirus to regulate cellular gene expression at the translational level may be an important mechanism that contributes to viral pathogenesis [32].

Similar to the results of the present study, proteins encoded by many viruses are known to interact with DNA-damage sensing and repair machinery because the viral integration process includes a DNA-repair step [10]. Among them, adenoviral E4orf6, the 34-kDa gene product of the E4 gene, interacts with DNA-PK and prolongs the signaling of DNA-damage causing caspase-dependent and independent cell death [33]. Concerning DNA-PK, gene array studies revealed that HTLV-I Tax expressing cells display a reduced level of Ku80 mRNA as compared with controls, which could reduce the efficiency of DNA-damage repair leading to an increase in the genomic mutation frequency [28].

The observation of interactions between viruses and cellular DNA-repair proteins has not only uncovered new complexities in virus–host interactions, but is also reinforcing the view that viruses can reveal key regulators of cellular pathways through the proteins they interact with [2,34]. We demonstrated that the acinus and MCM2 proteins are associated with the host-specific enhancement of DNA-damage-induced apoptosis by gp70. Acinus has been identified as a new nuclear factor which induces apoptotic chromatin condensation after cleavage by caspase-3 without inducing DNA fragmentation. Immunodepletion experiments showed that the acinus protein is essential for apoptotic chromatin condensation *in vitro*, and an antisense study revealed that acinus is also important in the induction of apoptotic chromatin condensation in cells [35]. However, knockdown experiments revealed that loss of acinus inhibited DNA fragmentation but not chromatin condensation during apoptosis [36]. Thus, the functions of acinus in apoptosis are still controversial. Acinus is known to play a role in the regulation of apoptosis in erythroid cells [37].

The MCM2–7 complex is known to act as a replicative helicase during DNA synthesis and plays a central role in S-phase genome stability. MCM proteins are required for processive DNA replication and are a target of S-phase checkpoints [38]. MCM expression is up-regulated in proliferating cells, providing a diagnostic marker for both cancerous cells and cells with the potential to become malignant. Loss of MCM function generates lethal double-strand breaks at sites of DNA synthesis during replication elongation [39]. MCM2 is also known to activate ATM and ATR kinase activity through the generation of truncated forms of Cdc6. The activation kinetics are consistent with elevated cellular levels of p53 and mitochondrial levels of Bax leading to apoptosis [40]. Because the PIKK family enzymes seem to function redundantly with each other in the setting of DNA-repair at DNA-damage or retroviral integration sites [12,41], the details of the controlling mechanisms for activation of DNA-PK but not ATM or ATR by acinus and MCM2 as well as gp70 proteins should be clarified in a future study.

In the process of development and progression, tumors frequently develop resistance to radiotherapy and chemotherapy [42]. Most of the current research in cancer gene therapy (CGT) is aimed at its development as a novel form of targeted therapy that can be combined with other treatment modalities such as radiotherapy and chemotherapy through the selective enhancement of radiosensitivity and cytotoxicity in tumors compared with normal tissues. In the present study, we demonstrated the potential of CGT in combination with IR for the future.

On the other hand, in virus-induced diseases such as adult-T-cell leukemia/lymphoma (ATLL) and the neurodegenerative disease known as HTLV-associated myelopathy/tropical spastic paraparesis (HAM/TSP) which is caused by HTLV-I, several studies have shown that the apoptotic pathway is largely intact and can be reactivated to induce specific killing [43]. A better understanding of the molecular mechanisms employed by viruses to counteract cellular death pathways remains an important challenge for future therapies and the treatment of virus-associated diseases.

In conclusion, we demonstrated the ability of an exogenous protein to prominently facilitate the host-cellular apoptosis signaling pathway in the present study. This modification needed the contribution of specific proteins that were recruited in a host-specific manner. This novel pathway of apoptotic signaling could provide a target for cancer/disease therapy.

Acknowledgements

We thank Dr. Kaoru Tanaka of the National Institute of Radiological Sciences, Chiba for technical assistance. This work was supported by a grant-in-aid No. 17590337 from the Ministry of Education, Culture, Sports, Science, and Technology of Japan.

References

[1] Clarke P, DeBiasi RL, Goody R, Hoyt CC, Richardson-Burns S, Tyler KL. Mechanisms of reovirus-induced cell death and tissue injury: role of apoptosis and virus-induced perturbation of host-cell signaling and transcription factor activation. Viral Immunol 2005;18:89–115.
[2] Goff SP. Host factors exploited by retroviruses. Nature Rev Microbiol 2007;5:253–63.
[3] Lin Y, Brown L, Hedley DW, Barber DL, Benchimol S. The death-promoting activity of p53 can be inhibited by distinct signaling pathways. Blood 2002;100:3990–4000.
[4] Nishigaki K, Hanson C, Thompson D, Yugawa T, Ruscetti S. Activation of the Jun N-terminal kinase pathway by friend spleen focus-forming virus and its role in the growth and survival of friend virus-induced erythroleukemia cells. J Virol 2005;79:12752–62.
[5] Kelley LL, Koury MJ, Bondurant MC, Koury ST, Sawyer ST, Wickrema A. Survival or death of individual proerythroblasts results from differing erythropoietin sensitivities: a mechanism for controlled rates of erythrocyte production. Blood 1993;82:2340–52.
[6] Brown L, Benchimol S. The involvement of MAPK signaling pathways in determining the cellular response to p53 activation: cell cycle arrest or apoptosis. J Biol Chem 2006;281:3832–40.
[7] Löbrich M, Jeggo PA. The impact of a negligent G2/M checkpoint on genomic instability and cancer induction. Nature Rev Cancer 2007;7:861–9.
[8] Barlow C, Brown KD, Deng CX, Tagle DA, Wynshaw-Boris A. ATM selectively regulates distinct p53-dependent cell-cycle checkpoint and apoptotic pathways. Nature Genet 1997;17:453–6.
[9] Shiloh Y. ATM and related protein kinases: safeguarding genome integrity. Nature Rev Cancer 2003;3:155–68.
[10] Lilley CE, Schwartz RA, Weitzman MD. Using or abusing: viruses and the cellular DNA damage response. Trends Microbiol 2007;15:119–26.
[11] Skalka AM, Katz RA. Retroviral DNA integration and the DNA damage response. Cell Death Differ 2005;12(Suppl. 1):971–8.
[12] Hasegawa M, Yamaguchi S, Aizawa S, Ikeda H, Tatsumi K, Noda Y, et al. Resistance against Friend leukemia virus-induced leukemogenesis in DNA-dependent protein kinase (DNA-PK)-deficient *scid* mice associated with

Please cite this article in press as: Hasegawa M, et al. A novel role for acinus and MCM2 as host-specific signaling enhancers of DNA-damage-induced apoptosis in association with viral protein gp70. Leuk Res (2008), doi:10.1016/j.leukres.2008.10.025

defective viral integration at the *Spi-1* and *Fli-1* site. Leuk Res 2005;29:933–42.
[13] Kitagawa M, Yamaguchi S, Hasegawa M, Tanaka K, Sado T, Hirokawa K, et al. Friend leukemia virus infection enhances DNA damage-induced apoptosis of hematopoietic cells, causing lethal anemia in C3H hosts. J Virol 2002;76:7790–8.
[14] Yamaguchi S, Hasegawa M, Aizawa S, Tanaka K, Yoshida K, Noda Y, et al. DNA-dependent protein kinase enhances DNA damage-induced apoptosis in association with Friend gp70. Leuk Res 2005;29:307–16.
[15] Banin S, Moyal S, Shieh SY, Taya Y, Anderson CW, Chessa L, et al. Enhanced phosphorylation of p53 by ATM in response to DNA damage. Science 1998;281:1674–7.
[16] Kitagawa M, Aizawa S, Kamisaku H, Ikeda H, Hirokawa K, Sado T. Cell-free transmission of Fv-4 resistance gene product controlling Friend leukemia virus-induced leukemogenesis: a unique mechanism for interference with viral infection. Blood 1995;86:1557–63.
[17] Kitagawa M, Aizawa S, Kamisaku H, Sado T, Ikeda H, Hirokawa K. Distribution of *Fv-4* resistant gene product in Friend leukemia virus-resistant *Fv-4r* mouse strain. Exp Hematol 1996;24:1423–31.
[18] Yugawa T, Amanuma H. Sequence flexibility in the polytropic env gp70-derived region of the membrane glycoprotein (gp55) of Friend spleen focus-forming virus affects its biological activity. J Virol 1998;72:2272–9.
[19] Noyce RS, Collins SE, Mossman KL. Identification of a novel pathway essential for the immediate-early, interferon-independent antiviral response to enveloped virions. J Virol 2006;80:226–35.
[20] Wang Y, Li H, Tang Q, Maul GG, Yuan Y. Kaposi's sarcoma-associated herpesvirus *ori-Lyt*-dependent DNA replication: involvement of host cellular factors. J Virol 2008;82:2867–82.
[21] Weterings E, Chen DJ. DNA-dependent protein kinase in nonhomologous end joining: a lock with multiple keys? J Cell Biol 2007;179:183–6.
[22] Tanaka K, Watanabe K, Yamaguchi S, Hasegawa M, Kitagawa M, Aizawa S. Cytological basis for enhancement of radiation-induced mortality by Friend leukaemia virus infection. Int J Radiat Biol 2004;80:673–81.
[23] Kitagawa M, Kamisaku H, Sado T, Kasuga T. Friend leukemia virus induced leukemogenesis in fully H-2 incompatible C57BL/6 → C3H radiation bone marrow chimeras. Leukemia 1993;7:1041–6.
[24] Kitagawa M, Aizawa S, Kamisaku H, Hirokawa K, Ikeda H. Protection of retrovirus-induced disease by transplantation of bone marrow cells transduced with MuLV *env* gene via retrovirus vector. Exp Hematol 1999;27:234–41.
[25] Shangary S, Brown KD, Adamson AW, Edmonson S, Ng B, Pandita TK, et al. Regulation of DNA-dependent protein kinase activity by ionizing radiation-activated Abl kinase is an ATM-dependent process. J Biol Chem 2000;275:30163–8.
[26] Westphal D, Ledgerwood EC, Hibma MH, Fleming SB, Whelan EM, Mercer AA. A novel Bcl-2-like inhibitor of apoptosis is encoded by the parapoxvirus ORF virus. J Virol 2007;81:7178–88.
[27] Thomson BJ. Viruses and apoptosis. Int J Exp Pathol 2001;82:65–76.
[28] Marriott SJ, Semmes OJ. Impact of HTLV-I Tax on cell cycle progression and the cellular DNA damage repair response. Oncogene 2005;24:5986–95.
[29] Höllsberg P. Mechanisms of T-cell activation by human T-cell lymphotropic virus type I. Microbiol Mol Biol Rev 1999;63:308–33.
[30] Beutler B, Eidenschenk C, Crozat K, Imler JL, Takeuchi O, Hoffmann JA, et al. Genetic analysis of resistance to viral infection. Nature Rev Immunol 2007;7:753–66.
[31] Zhao X, Yoshimura FK. Expression of murine leukemia virus envelope protein is sufficient for the induction of apoptosis. J Virol 2008;82:2586–9.
[32] Yoshimura FK, Luo X, Zhao X, Gerard HC, Hudson AP. Up-regulation of a cellular protein at the translational level by a retrovirus. Proc Natl Acad Sci USA 2008;105:5543–8.
[33] Hart LS, Ornelles D, Koumenis C. The adenoviral E4orf6 protein induces atypical apoptosis in response to DNA damage. J Biol Chem 2007;282:6061–7.
[34] Nolan D, Gaudieri S, Mallal S. Host genetics and viral infections: immunology taught by viruses, virology taught by the immune system. Curr Opin Immunol 2006;18:413–21.
[35] Sahara S, Aoto M, Eguchi Y, Imamoto N, Yoneda Y, Tsujimoto Y. Acinus is a caspase-3-activated protein required for apoptotic chromatin condensation. Nature 1999;401:168–73.
[36] Joselin AP, Schulze-Osthoff K, Schwerk C. Loss of Acinus inhibits oligonucleosomal DNA fragmentation but not chromatin condensation during apoptosis. J Biol Chem 2006;281:12475–84.
[37] Testa U. Apoptotic mechanisms in the control of erythropoiesis. Leukemia 2004;18:1176–99.
[38] Bailis JM, Forsburg SL. MCM proteins: DNA damage, mutagenesis and repair. Curr Opin Genet Dev 2004;14:17–21.
[39] Bailis JM, Luch DD, Hunter T, Forsburg SL. Minichromosome maintenance proteins interact with checkpoint and recombination proteins to promote s-phase genome stability. Mol Cell Biol 2008;28:1724–38.
[40] Yim H, Hwang IS, Choi JS, Chun KH, Jin YH, Ham YM, et al. Cleavage of Cdc6 by caspase-3 promotes ATM/ATR kinase-mediated apoptosis of HeLa cells. J Cell Biol 2006;174:77–88.
[41] Smith JA, Wang FX, Zhang H, Wu KJ, Williams KJ, Daniel R. Evidence that the Nijmegen breakage syndrome protein, an early sensor of double-strand DNA breaks (DSB), is involved in HIV-1 post-integration repair by recruiting the ataxia telangiectasia-mutated kinase in a process similar to, but distinct from, cellular DSB repair. Virol J 2008;5:11.
[42] Hingorani M, White CL, Agrawal VK, Vidal L, Melcher A, Harrington KJ. Combining radiation and cancer gene therapy: a potential marriage of physical and biological targeting? Curr Cancer Drug Targets 2007;7:389–409.
[43] Taylor JM, Nicot C. HTLV-1 and apoptosis: role in cellular transformation and recent advances in therapeutic approaches. Apoptosis 2008;13:733–47.

Please cite this article in press as: Hasegawa M, et al. A novel role for acinus and MCM2 as host-specific signaling enhancers of DNA-damage-induced apoptosis in association with viral protein gp70. Leuk Res (2008), doi:10.1016/j.leukres.2008.10.025

bjh research paper

Angiogenic mediators of the angiopoietin system are highly expressed by CD10-positive lymphoma cells in angioimmunoblastic T-cell lymphoma

Klio Konstantinou,[1,2] Kouhei Yamamoto,[1] Fumiaki Ishibashi,[1] Yuiko Mizoguchi,[1] Morito Kurata,[1] Yasunori Nakagawa,[3] Kenshi Suzuki,[3] Motoji Sawabe,[4] Masatsugu Ohta,[5] Shigesaburo Miyakoshi,[5] James T. Crawley[2] and Masanobu Kitagawa[1]

[1]Department of Comprehensive Pathology, Ageing and Developmental Sciences, Graduate School, Tokyo Medical and Dental University, Tokyo, Japan, [2]Department of Haematology, Imperial College of London, London, UK, [3]Department of Haematology, Japanese Red Cross Medical Centre, and Departments of [4]Pathology and [5]Haematology, Tokyo Metropolitan Geriatric Hospital, Tokyo, Japan

Received 28 August 2008; accepted for publication 6 November 2008

Correspondence: Masanobu Kitagawa, MD, Department of Comprehensive Pathology, Ageing and Developmental Sciences, Graduate School, Tokyo Medical and Dental University, 1-5-45 Yushima, Bunkyo-ku, Tokyo 113-8519, Japan. E-mail: masa.pth2@tmd.ac.jp

Summary

Angioimmunoblastic T-cell lymphoma (AILT) is a malignant disease of peripheral T-cell origin that is characterized by a prominent proliferation of high endothelial venules in the lymph node. To investigate angiogenic mechanisms in AILT we measured the angiogenic mediator gene expression levels in the lymph nodes of 54 non-Hodgkin lymphoma patients, by immunostaining and quantitative reverse transcription polymerase chain reaction. Angiogenic mediators angiopoietin (Ang) 1 (*ANGPT1*), Ang2 (*ANGPT2*) and their receptor, Tie2 (*TEK*), vascular endothelial growth factor (VEGF; *VEGFA*) and its receptor, VEGFR2 (*KDR*), and hepatocyte growth factor (*HGF*) and its receptor, c-Met (*MET*) were all more highly expressed in AILT lymph nodes (16 cases) than in B-cell lymphomas (24 cases). Moreover, significantly higher Ang1 and Tie2 expression was detected in AILT cases with CD10-positive neoplastic T-cells by comparison with unspecified peripheral T-cell lymphoma (14 cases). Immunostaining confirmed the expression of Ang1 and VEGF by both neoplastic T-cells and follicular dendritic cells. These results suggest that the angiopoietin system may play an important role in the development of high vascularity in AILT lymph nodes. Consequently, as neoplastic T-cells and follicular dendritic cells are both increased in AILT and may represent an important source of angiogenic mediators, targeting these cells with anti-angiogenic strategies might represent a novel therapy for AILT.

Keywords: angioimmunoblastic T-cell lymphoma, angiogenesis, angiopoietin, VEGF, follicular dendritic cell.

Angiogenesis is the process of generation of new blood vessels from a pre-existing capillary network (Yancopoulos *et al*, 2000). As both cell function and survival are critically dependent on the supply of oxygen and nutrients, all cells must reside within 100 μm of a capillary. In adult tissues, angiogenesis is tightly regulated, with most blood vessels remaining quiescent and angiogenesis only occurring in the female reproductive system and during wound healing and tissue repair. Such vascular quiescence in normal tissues is maintained by a delicate balance between angiogenic activators and inhibitors. Alterations in this balance can re-activate angiogenesis because endothelial cells retain the ability to divide (Carmeliet, 2003; Ribatti *et al*, 2007a). Conditions in which angiogenesis is known to be inappropriately switched on include various malignant, ocular and inflammatory disorders (Carmeliet, 2005). Currently, it is thought that both solid and haematological tumours are capable of switching on angiogenesis and that their growth, invasion and metastasis are angiogenesis-dependent upon this (Ribatti *et al*, 1999; Bazarbachi *et al*, 2004). Angiogenesis is an adverse prognostic indicator in several solid tumours. Furthermore, recent data suggest that angiogenesis also plays an important role in the evolution of haematological malignancies (Lim & Levine, 2005; Keith *et al*, 2007).

Angioimmunoblastic T-cell lymphoma (AILT) is an uncommon type of non-Hodgkin lymphoma (NHL)

First published online 16 December 2008
doi:10.1111/j.1365-2141.2008.07534.x

characterized by systemic disease, and a polymorphous infiltrate involving lymph nodes with a prominent proliferation of high endothelial venules and follicular dendritic cells (FDCs) (Jaffe *et al*, 2001; Attygalle *et al*, 2002; Merchant *et al*, 2006). The neoplastic T-cells are detected by a clear cytoplasm with distinct cell membranes and are typically found in the paracortex clustered around blood vessels (Ferry, 2002). Neoplastic T-cells are CD4-positive in the majority of AILT cases (Dunleavy *et al*, 2007). However, CD10 in these cells has also been suggested as a marker of AILT, and the expression of *MME* (CD10) mRNA in the neoplastic cellular component has recently been confirmed (Attygalle *et al*, 2002; Merchant *et al*, 2006; de Leval *et al*, 2007). A subset of AILT cells has also been shown to express Bcl-6 (de Leval *et al*, 2001). Given that both CD10 and Bcl-6 are known as markers of follicular helper T (T_{FH}) cells (Piccaluga *et al*, 2007), their expression on AILT neoplastic T-cells confers a unique phenotype that suggests these cells are of germinal centre origin.

Synthesis of angiogenic factors, such as vascular endothelial growth factor (VEGF), by neoplastic cells in NHL cases has been demonstrated in a number of studies (Foss *et al*, 1997; Bellamy *et al*, 1999; Zhao *et al*, 2004). Fibroblasts in the stroma, and immune cells, such as macrophages and mast cells, are all capable of producing angiogenic peptides in haematological malignancies (Mangi & Newland, 2000; Moehler *et al*, 2003). It has therefore been suggested that neoplastic haematological cells, tumour stromal cells and immune cells might form part of a positive regulatory feedback loop that promotes angiogenesis and, consequently, also haematological tumour cell growth (Moehler *et al*, 2003).

VEGFA expression was detected in the lymph node of AILT patients by *in situ* hybridization (Foss *et al*, 1997). Subsequently, Zhao and colleagues used the laser microdissection technique and quantitative PCR method to detect *VEGFA* mRNA in both neoplastic and endothelial cells in AILT (Zhao *et al*, 2004). In their study, increased levels of *VEGFA* gene expression in lymphoma and endothelial cells were related to both extranodal involvement and poor prognosis. The production of VEGF by neoplastic cells in AILT was recently confirmed by immunohistochemical studies (Piccaluga *et al*, 2007).

Despite these recent data, it must be considered that the regulation of angiogenesis is complex. Consequently, additional positive and negative mediators might contribute to the angiogenic switch in the lymph node of AILT cases, especially in the advanced stage. An improved understanding of the angiogenic mechanisms that are operating in AILT will increase current knowledge of the biology of disease and also provide insights into new treatments that are likely to improve the existing poor clinical outcome of AILT patients. To this end, we undertook a systematic analysis of microvascular density (MVD) and the expression of angiogenic mediators in the lymph node of AILT and other NHL cases.

Materials and methods

Patients

Formalin-fixed, paraffin-embedded and fresh frozen lymph node specimens from 54 NHL cases were obtained from the Tokyo Medical and Dental University Hospital, the Tokyo Metropolitan Geriatric Hospital and the Japanese Red Cross Medical Centre, Tokyo, Japan. Formalin-fixed, paraffin-embedded lymph node samples were used for diagnosis as well as immunohistochemical analysis and fresh frozen samples were used for quantification of gene expression. Samples included: 16 AILT (of which six were CD10-positive) [male:female, 9:7; age, median 72 years (range, 42–87 years)] specimens, 14 peripheral T-cell lymphoma, unspecified [PTCLu; male:female, 7:7; age, median 66 years (range, 31–95 years)] specimens, 9 diffuse large B cell lymphoma [DLBCL; male:female, 8:1; age, median 78 years (range, 62–84 years)] specimens and 15 follicular lymphoma [FL; male:female, 4:11; age, median 59 years (range, 48–73 years)] specimens. Diagnosis in each case was based on standard histological criteria and clinical and laboratory findings according to the World Health Organization classification (Jaffe *et al*, 2001) and was performed by at least two experienced pathologists. All specimens were obtained at the time of initial diagnosis. The patients were not infected with specific viruses, including human T cell leukaemia virus type 1 and had not been treated with specific therapeutic drugs prior to the study. Furthermore, six peripheral blood samples obtained from healthy volunteers were used as negative controls. Informed consent was obtained from all individuals. This study was approved by the ethical committee of the Tokyo Metropolitan Geriatric Hospital.

Detection of CD3 and CD10 in AILT lymph nodes

In AILT lymph nodes, CD10-positive neoplastic T-cells were identified by double immunostaining using rabbit polyclonal anti-CD3 (DAKO, Glostrup, Denmark) and mouse monoclonal anti-CD10 antibody (Novocastra Laboratories Ltd, Newcastle, UK) as described previously (Keith *et al*, 2007), and using 3,3′ diaminobenzidine (DAB) (Nichirei, Tokyo, Japan) to detect CD10, and 3-amino-9-ethylcarbazole (AEC, DAKO) for CD3.

Preparation of RNA and quantitative reverse transcription polymerase chain reaction (RT-PCR)

RNA was extracted from frozen lymph node specimens of both malignant lymphoma and control subjects as previously described (Yamamoto *et al*, 2004). For quantitative RT-PCR, fluorescent hybridization probes and the TaqMan PCR Core Reagents Kit with AmpliTaq Gold (PerkinElmer Cetus, Norwalk, CT, USA) were used with the ABI Prism 7900HT Sequence Detection System (PerkinElmer). Oligonucleotides (as specific primers) and TaqMan probes for the angiogenic mediators angiopoietin-1 (*ANGPT1*) (Abdel-Malak *et al*,

2008), angiopoietin-2 (*ANGPT2*) (Harfouche & Hussain, 2006), VEGF (*VEGFA*) (Ferrara *et al*, 2003), hepatocyte growth factor (*HGF*) (Zhang *et al*, 2003), basic fibroblast growth factor (*FGF2*) (Ribatti *et al*, 2007b), tumour necrosis factor-α (*TNF*) (Yoshida *et al*, 1997), transforming growth factor-β (*TGFB1*) (Elliott & Blobe, 2005) and the receptors Tie2 (*TEK*) (Abdel-Malak *et al*, 2008), VEGFR2 (*KDR*) (Ferrara *et al*, 2003) and c-Met (*MET*) (Zhang *et al*, 2003), all thought to be surrogate markers of angiogenesis, and glyceraldehyde-3-phosphate dehydrogenase (*GAPDH*) mRNA were synthesized at a commercial laboratory (PerkinElmer Cetus). The sequences of primers and TaqMan probes are summarized in Table I. Conditions for the one-step RT-PCR were as follows: 30 min at 48°C, 10 min at 95°C and then 40 cycles of amplification for 15 s at 95°C and 1 min at 60°C. The expression of angiogenic mediators was quantified according to our previously described method (Yamamoto *et al*, 2004). Briefly, the intensity of the reaction was evaluated from the quantity of total RNA in HeLa cells (ng) corresponding to the initial number of PCR cycles to reveal the linear increase in reaction intensity (threshold cycle) for each sample on a logarithmic standard curve. The quantities of RNA (ng) for the different angiogenic mediators were normalized using the data for *GAPDH* in each sample using the $2^{-\Delta\Delta CT}$ method (Livak & Schmittgen, 2001).

Double immunostaining for angiogenic mediators and cell marker

The study of the distribution of angiogenic mediators in the lymph node of AILT cases was performed by double immunostaining. For this, 4 μm-thick formalin-fixed tissue sections were treated with 0·3% hydrogen peroxide in methanol to quench endogenous peroxidase activity and blocked with either 10% normal goat or rabbit serum, as appropriate. Thereafter, either a polyclonal goat anti-Ang1 (Santa Cruz Biotechnology Inc., Santa Cruz, CA, USA) or rabbit polyclonal anti-VEGF (Santa Cruz Biotechnology Inc.) were applied. Sections were washed and then incubated with rabbit anti-goat or goat anti-rabbit IgG (DAKO) followed by a peroxidase-conjugated streptavidin system (DAKO) with DAB as the chromogen. Following colour development, sections were treated with 0·1% trypsin in Tris buffer, quenched and blocked as before, and then incubated with either mouse monoclonal anti-CD3 antibody (T-cell marker) (DAKO), anti-CD10 antibody, or anti-CD21 antibody (FDC marker) (DAKO). Sections were finally incubated with goat anti-mouse IgG antibody followed by a peroxidase-conjugated streptavidin system using either AEC or nickel DAB (Vector Laboratories, Burlingame, CA, USA) as the chromogen.

Statistical analysis

Statistically significant differences in the quantitative analysis of mRNA expression were calculated using SPSS statistical software (SPSS Inc., Chicago, IL, USA). The *P*-values were calculated using the Mann–Whitney's *U*-test corrected by the sequentially rejective Bonferroni method, and were considered significant when $P < 0{\cdot}05$.

Table I. Primers and probes for real-time RT-PCR used in the study.

Mediators	Sequences
VEGFA	
Forward primer	GACCGCGACTCGGAGAGATG
Reverse primer	ATGTCCCTACTCCTGTGGCC
Probe	GGTCCAGTCTGCCTGTCTTTCTGTCTAGT
NUDT6	
Forward primer	GCCGTACATCGAGTACTAGATAC
Reverse primer	TCACTCGTTTAGACGGGACG
Probe	ACAAAGATACA GCACCTTCGT
TNF	
Forward primer	GCTCAGACCCGTCCAGATGAAA
Reverse primer	AGGTTGGAAGGGTTTGCG
Probe	AGTAACGGGACACTCCTCCTGCTTGT
HGF	
Forward primer	CTCCGGTACCACGATATGAGAAC
Reverse primer	CGTTAATTTTGT ACGCGACTGT
Probe	GGGAGTGT GGGCGACCCTCATGACT
TGFB1	
Forward primer	GAGAGGCTGGACGGTGTCT
Reverse primer	TCTAGCGCGGGTAGATCCAA
Probe	GGGATAAGTTCTGGTGGGTGGAAGACCA
ANGPT1	
Forward primer	TCACATAGGGTGCAGCAATCAG
Reverse primer	GT AGGCACATTGCCCATGTTG
Probe	CCGAAGTCCAGAAAACAGTGGGAGAAGA TATAAC
ANGPT2	
Forward primer	TTCCT CCTGCCAGAGATGGA
Reverse primer	TGCACAGCATTGGACACGTA
Probe	AACTGCCGCTCTTCCTCCAGCCC
TEK	
Forward primer	ACTTCGGTGCTACTTAACAACTTACATC
Reverse primer	CCTGGGCCTTGGTGTTGAC
Probe	CAGGGAGCAGTACGTGGTCCGAGCT
KDR	
Forward primer	CACCACTCAAACGCTGACATGTA
Reverse primer	CCAACTGCCAATACCAGTGGAT
Probe	TGCCATTCCTCCCCCGCATC
MET	
Forward primer	CTGTTTACTTGTTGCAAGGGAGGA
Reverse primer	TAGGGTGCCAGCATTTTAGCA
Probe	ACTCCTACAACCCGAATACTGCCCAGACC

Results

CD10-positive phenotype of neoplastic T-cells in AILT cases

In six of the 16 AILT cases (38%), CD10 was detected on the cell surface of neoplastic T-cells. In these cases, both CD3

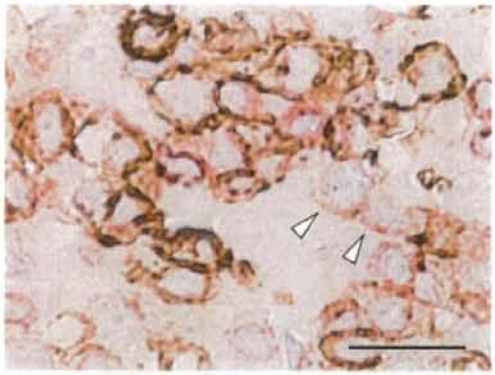

Fig 1. Double immunostaining for CD3 (red) and CD10 (brown) in the lymph node of an AILT case. In this CD10-positive AILT case, a proportion of neoplastic T-cells were double-positive for CD3 and CD10. Note both the cytoplasmic/cell surface positive reaction for CD3 (red) and cell surface staining for CD10 (brown) in relatively large cells. Of all the large neoplastic cells, some are only positive for CD3 (red) (white arrowheads). Scale bar in figure indicates 50 μm in length.

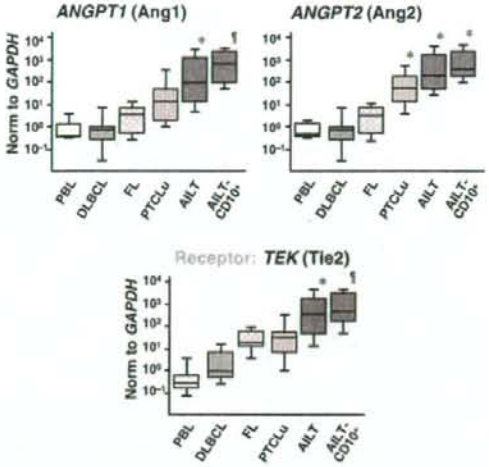

Fig 2. Expression of angiogenic mediators in PBL (control), the lymph node of DLBCL, FL, PTCLu, AILT and AILT-CD10$^+$ cases, as determined by quantitative RT-PCR. These box plots compare the levels of mRNA expression for angiopoietin system molecules including *ANGPT1*, *ANGPT2*and *TEK*. Bars indicate 90%-tile and 10%-tile and boxes indicate 75%-tile to 25%-tile with lines of median values inside the boxes. Differences were significant between *ANGPT1*expression levels in PBL/DLBCL/FL and AILT (*$P < 0{\cdot}0001$) and PTCLu and AILT-CD10$^+$ (¶$P < 0{\cdot}01$). Significant differences were also observed between *ANGPT2* expression levels in PBL/DLBCL/FL and PTCLu/AILT/AILT-CD10$^+$ (*$P < 0{\cdot}001$) and between *TEK* expression levels in PBL/DLBCL/FL and AILT (*$P < 0{\cdot}01$), and PTCLu and AILT-CD10$^+$ (¶$P < 0{\cdot}01$).

(cytoplasm and cell surface) and CD10 (cell surface) antigens were detected by double immunostaining in relatively large neoplastic T-cells (Fig 1). Some CD3-positive (CD10-negative) neoplastic T-cells were also identified (Fig 1, white arrowheads). According to previous immunohistochemical studies in AILT lymph node specimens (Attygalle *et al*, 2002), CD10-positive neoplastic T-cells represent a small proportion of T-cells (5–30%). To rule out the mixture of non-neoplastic scattered normal follicular helper T-cells that express CD3 and CD10, the significant proliferation of CD10-positive neoplastic T cells should be determined. For this reason, the threshold for classification as CD10-positive in our study was set at 10% of all CD3-positive T-cells.

Expression of angiogenic mediators

Expression levels of 10 positive mediators of angiogenesis were studied by quantitative PCR in each of cDNA samples prepared from lymph node sections of 54 cases with NHL and in six negative control samples (PBL). Expression levels were grouped according to lymphoma subtype (DLBCL, FL, PTCLu, AILT) and data for the AILT cases was further divided into two groups: AILT (overall) and AILT CD10-positive (the former group included cases with both CD10-positive and CD10-negative neoplastic T-cells).

The factors of the angiopoietin system investigated included Ang1, Ang2 and their receptor Tie2, which were all considered together in gene expression analysis due to their inter-related angiogenic roles. In general, the highest levels of expression of all angiogenic mediators were seen in AILT and CD10-positive cases (Fig 2). In contrast, DLBCL was shown to have the lowest expression levels among the lymphoma subtypes studied in this investigation. For *ANGPT1*, *ANGPT2* and *TEK*, statistically significant differences were found to exist between PTCLu, AILT and CD10-positive AILT and the control group. In the case of *TEK*, the difference in the expression between FL and the control group was also statistically significant. DLBCL had significantly lower expression levels than PTCLu, AILT and CD10-positive AILT. Furthermore, FL had significantly lower expressions of *ANGPT1*, *ANGPT2* and *TEK* than AILT and CD10-positive AILT. In the cases of *ANGPT1* and *ANGPT2*, statistically significant differences also existed between PTCLu and CD10-positive AILT. Factors of the VEGF system, including VEGFA and its receptor VEGFR2 (*KDR*), are shown in Fig 3. Expression levels of *VEGFA* were significantly higher in AILT and CD10-positive AILT than in DLBCL and FL. *KDR* was shown to be more highly expressed in AILT and CD10-positive AILT than DLBCL.

While angiopoietin and VEGF system mediators are specific angiogenic factors whose actions are mediated by endothelial receptors, HGF, bFGF, tumour necrosis factor-α (TNF-α) and transforming growth factor-β (TGF-β) are non-specific in their actions. As shown in Fig 4, expression levels of the factors of the HGF system, including *HGF* and *MET*, were significantly higher in AILT and CD10-positive AILT than in DLBCL

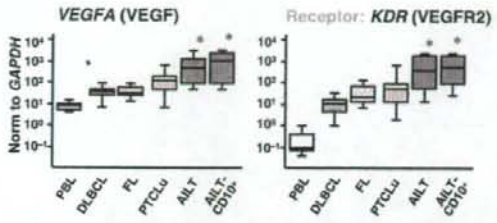

Fig 3. Expression of angiogenic mediators of VEGF system in PBL (control), the lymph node of DLBCL, FL, PTCLu, AILT and AILT-CD10$^+$ cases. Differences were significant between the *VEGFA* expression levels in PBL/DLBCL/FL and AILT/AILT-CD10$^+$ ($^*P < 0{\cdot}001$), and between the *KDR* expression levels in PBL/DLBCL and AILT/AILT-CD10$^+$ ($^*P < 0{\cdot}001$).

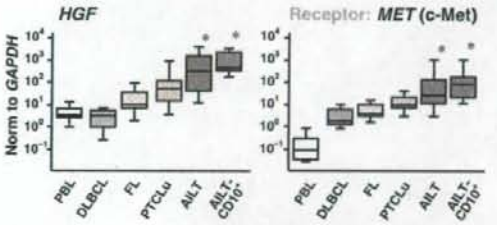

Fig 4. Expression of HGF system mediators in PBL (control), the lymph node of DLBCL, FL, PTCLu, AILT and AILT-CD10$^+$ cases. Differences were significant between *HGF* expression levels in PBL/DLBCL/FL and AILT/AILT-CD10$^+$ ($^*P < 0{\cdot}01$), and between *MET* expression levels in PBL/DLBCL/FL and AILT/AILT-CD10$^+$ ($^*P < 0{\cdot}001$).

and FL. The expression levels of other angiogenesis-associated factors are summarized in Fig 5. *FGF2* was significantly over-expressed in PTCLu, AILT, CD10-positive AILT and FL than in the control samples. DLBCL samples exhibited a significantly lower expression of *FGF2* than any other lymphoma subtype. *TNF* was more highly expressed in all lymphoma subtypes than in the control samples, but differences in expression between lymphoma subtypes were not significant. Expression levels of *TGFB1* were not significantly higher in any of the lymphoma subtypes compared with the control samples.

Localization of angiogenic mediators in the lymph node from AILT cases

To localize the major specific angiogenic mediators in AILT lymph nodes, as determined by RT-PCR analysis, double immunostaining was performed for Angl and VEGF, and cell markers. Angl was positive in the cytoplasm of slightly large round cells with irregularly distributed nuclear chromatin that were positive for CD3 (Fig 6C) and CD10 (Fig 6D). The finding suggested that Angl was mainly expressed in CD3-positive and CD10-positive neoplastic T-cells. Small round CD3-positive non-neoplastic T-cells as well as CD3-negative

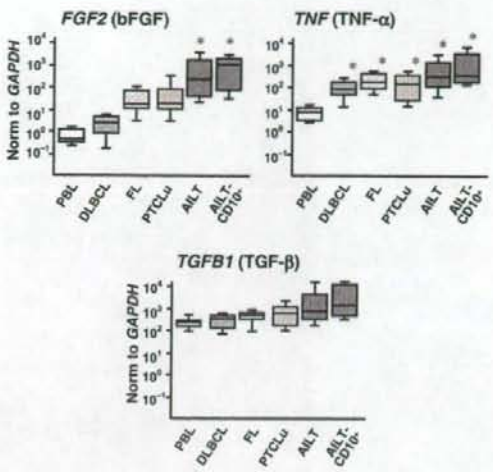

Fig 5. Expression of other non-specific angiogenic mediators in PBL (control), the lymph node of DLBCL, FL, PTCLu, AILT and AILT-CD10$^+$ cases. Differences were significant between *FGF2* expression levels in PBL/DLBCL and AILT/AILT-CD10$^+$ ($^*P < 0{\cdot}001$), and between *TNF* expression levels in PBL and NHL samples (DLBCL/FL/AILT/AILT-CD10$^+$) ($^*P < 0{\cdot}001$).

B-cells were negative for Angl. In addition, irregular shaped large cells were positively stained for Angl (Fig 6B). These cells were CD21-positive (Fig 6E and F) indicating that FDCs in AILT lymph nodes also produced Angl.

Figure 7 shows the localization of VEGF in the lymph node of AILT cases. Double immunostaining indicated that the majority of VEGF positive cells were relatively large in size and also positive for CD3 antigen, suggesting that these cells were neoplastic T-cells. Some areas of the vascular endothelial lining exhibited a weakly positive reaction for VEGF (black arrows, Fig 7A). VEGF was also positively stained in scattered large cells with abundant cytoplasm that were CD3-negative (white arrowheads, Fig 7A). Furthermore, the majority of CD10-positive cells were positively stained for VEGF (Fig 7B). As shown in Fig 7C, double immunostaining revealed that CD21-positive meshwork-like patterns of FDCs were also partly positive for VEGF. The CD3-negative large cells with VEGF expression were mostly positive for CD21, with the double-stained dark colour showing as a mixture of brown and bluish grey (black arrowheads, Fig 7D). Therefore, neoplastic T-cells and also FDCs in AILT lymph nodes may contribute to the production of VEGF.

Discussion

In recent years, our greater understanding of angiogenic mechanisms operating in haematologic malignancies has led to a growing interest in the testing of anti-angiogenic therapies. Despite this, the angiogenic mechanisms that occur in the

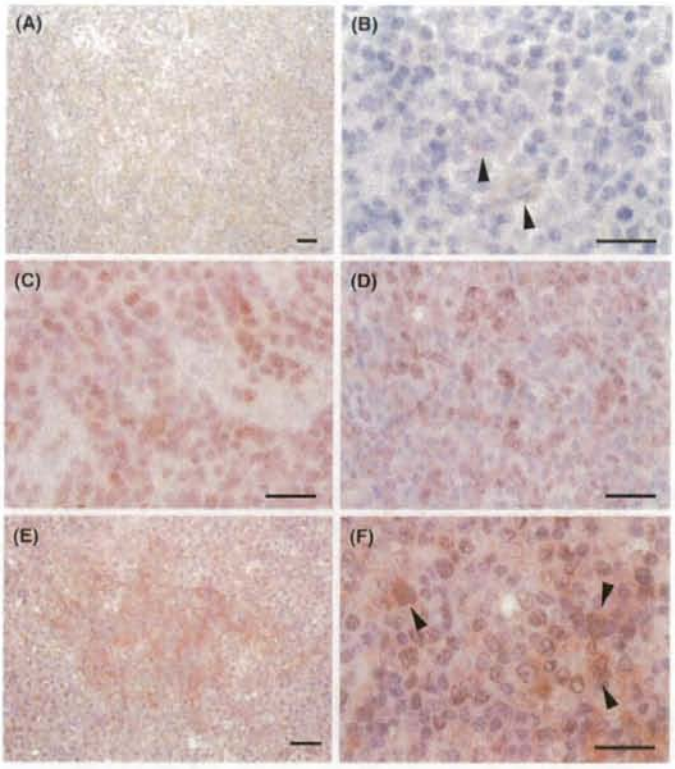

Fig 6. Immunohistochemical localization of Ang1 in the lymph node of AILT cases. Immunohistochemical staining for Ang1 showing positive reaction in the neoplastic cells of perivascular areas (A, counterstained with haematoxylin) and also in the irregular-shaped large cells (B, counterstained with haematoxylin). Microscopic features by double immunostaining for Ang1 (brown) and T-cell marker, CD3 (red) (C, counterstained with haematoxylin), for Ang1 (brown) and neoplastic cell marker, CD10 (red) (D, counterstained with haematoxylin), and for Ang1 (brown) and FDC marker, CD21 (red) (E, counterstained with haematoxylin; F, counterstained with haematoxylin) are shown. The CD21 antigen showing meshwork-pattern distribution in the AILT lymph node (E, red). Note the double positive reactions for Ang1 and CD3 as well as CD10 in neoplastic T-cells (C and D, brownish dark red) and for Ang1 and CD21 in FDC-like irregular-shaped large cells in AILT (F, brownish dark red) (black arrowheads). Scale bars in figures indicate 50 μm in length.

lymph nodes of AILT patients remain poorly understood. It has been known for some time that amongst the lymphomas, AILT patients exhibit the greatest neovascularization (Jaffe *et al*, 2001). In our study, MVD in AILT lymph nodes was approximately two-fold higher than in PTCLu and DLBCL. The observation that T-cell lymphomas have significantly higher MVD than DLBCL and FL is also supported by another recent study (Jorgensen *et al*, 2007). Interestingly, despite similarities in the pathophysiology of these two nodal T-cell lymphomas a significantly higher MVD was observed in AILT than in PTCLu. This perhaps supports the hypothesis that angiogenesis is particularly important for the pathophysiology of AILT, potentially making it an excellent candidate for anti-angiogenic therapy.

The angiopoietin, VEGF, and HGF systems are likely to play a key role in AILT angiogenesis, particularly in light of our gene expression analyses in CD10-positive cases of AILT. The expression levels of Ang1, Ang2 and HGF in B-cell lymphomas were low and not significantly different from the expression levels in the control samples. It is thus perhaps reasonable to suggest that the angiogenic factors involved in AILT are distinct from those associated with angiogenesis in DLBCL or FL. Although AILT exhibited the highest expression levels of angiogenic factors and receptors among all subtypes of malignant lymphoma examined, the differences were not significant between AILT and PTCLu. This may imply that the angiogenic mechanisms in the two nodal T-cell lymphomas are similar. However, the finding that Ang1 and Tie2 were expressed significantly higher in the CD10-positive AILT than in PTCLu cases suggests that distinct angiogenic mechanisms may be taking place in AILT. The frequency of CD10-positive AILT out of the total number of AILT cases was rather low in

